






















HD 83443c: A highly eccentric giant planet on a 22-year orbit

ADRIANA ERRICO ¹ ROBERT A. WITTENMYER ¹ JONATHAN HORNER ¹ ZHEXING LI ² G. MIREK BRANDT ^{3, *}
STEPHEN R. KANE ² TARA FETHEROLF ^{2, †} TIMOTHY R. HOLT ^{1, 4} BRAD CARTER ¹ JAKE T. CLARK ¹
R.P. BUTLER ⁵ C.G. TINNEY ⁶ SARAH BALLARD ⁷ BRENDAN P. BOWLER ⁸ JOHN KIELKOPF ⁹ HUIGEN LIU,¹⁰
PETER P. PLAVCHAN ¹¹ AVI SHPORER ¹² HUI ZHANG ¹³ DUNCAN J. WRIGHT ¹ BRETT C. ADDISON ¹
MATTHEW W. MENGEL ¹ AND JACK OKUMURA¹

¹University of Southern Queensland, Centre for Astrophysics, West Street, Toowoomba, QLD 4350 Australia

²Department of Earth and Planetary Sciences, University of California, Riverside, CA 92521, USA

³Department of Physics, University of California, Santa Barbara, Santa Barbara, CA 93106, USA

⁴Department of Space Studies, Southwest Research Institute, Boulder, CO, USA

⁵Department of Terrestrial Magnetism, Carnegie Institution of Washington, 5241 Broad Branch Road, NW, Washington, DC 20015-1305, USA

⁶Exoplanetary Science at UNSW, School of Physics, UNSW Sydney, NSW, 2052, Australia

⁷Department of Astronomy, University of Florida, 211 Bryant Space Science Center, Gainesville, FL, 32611, USA

⁸Department of Astronomy, The University of Texas at Austin, TX 78712, USA

⁹Department of Physics and Astronomy, University of Louisville, Louisville, KY 40292, USA

¹⁰School of Astronomy and Space Science, Key Laboratory of Modern Astronomy and Astrophysics in Ministry of Education, Nanjing University, Nanjing 210046, Jiangsu, China

¹¹Department of Physics and Astronomy, George Mason University, 4400 University Drive, Fairfax, VA 22030, USA

¹²Department of Physics and Kavli Institute for Astrophysics and Space Research, Massachusetts Institute of Technology, Cambridge, MA 02139, USA

¹³Shanghai Astronomical Observatory, Chinese Academy of Sciences, Shanghai 200030, China

Submitted to Astronomical Journal

ABSTRACT

We report the discovery of a highly eccentric long-period Jovian planet orbiting the hot-Jupiter host HD 83443. By combining radial velocity data from four instruments (AAT/UCLES, Keck/HIRES, HARPS, Minerva-Australis) spanning more than two decades, we find evidence for a planet with $m \sin i = 1.35_{-0.06}^{+0.07} M_{\text{J}}$, moving on an orbit with $a = 8.0 \pm 0.8$ au and eccentricity $e = 0.76 \pm 0.05$. We combine our radial velocity analysis with *Gaia* eDR3 /*Hipparcos* proper motion anomalies and derive a dynamical mass of $1.5_{-0.2}^{+0.5} M_{\text{Jup}}$. We perform a detailed dynamical simulation that reveals locations of stability within the system that may harbor additional planets, including stable regions within the habitable zone of the host star. HD 83443 is a rare example of a system hosting a hot Jupiter and an exterior planetary companion. The high eccentricity of HD 83443c suggests that a scattering event may have sent the hot Jupiter to its close orbit while leaving the outer planet on a wide and eccentric path.

Keywords: Planet hosting stars(1242) – Radial velocity(1332) – Exoplanet astronomy(486) – Exoplanet dynamics(490) – Subgiant stars(1646) – Astrometry(80)

1. INTRODUCTION

Corresponding author: Adriana Errico

Adriana.Errico@usq.edu.au

* NSF Graduate Research Fellow

† UC Chancellor’s Fellow

Thirty years ago the only planetary system known was the Solar System. We now know of thousands of exoplanets¹, and have learned that such worlds are far more diverse than we ever expected based on our system. Despite this great unveiling, we have yet to discover the true place of the Solar system among its siblings. Is the Solar system’s architecture common, or unusual? Are planetary systems like our own rare, or the norm?²

Because of the challenges involved in finding Earth-sized planets on Earth-like orbits around Sun-like stars (e.g. [Endl et al. 2015](#)), a key focus of current research efforts is the search for, and study of, Jupiter- and Saturn analogues – planets similar to the Solar system’s two gas giants, moving on similar, long-period orbits (e.g. [Zechmeister et al. 2013](#); [Wittenmyer et al. 2014](#); [Rowan et al. 2016](#); [Wittenmyer et al. 2016, 2017b](#); [Fulton et al. 2021](#)). The study of such objects can provide vital clues as to the degree to which the Solar system is unusual, helping to place our own planetary system in the context of the wider population. Whilst the scientific value of such Solar system analogues is high, they remain challenging to detect, with the main exoplanet detection methods being strongly biased towards the discovery of planets in systems that are not like our own (see e.g. [Perryman 2018](#), and references therein).

The formation of planets is a byproduct of the formation of stars. Vast clouds of dust and gas collapse, leading to the formation of a protostar, surrounded by a circumstellar disk from which the planets form (e.g. [Bodenheimer 1997](#); [Mannings et al. 2000](#); [Boss 2003](#)). Initially, those planets form through the collisional accumulation of successively larger bodies ([Wetherill 1990](#)). If this process takes longer than the typical lifetime of the gaseous component of the circumstellar disk, the resulting planets will be comparable to the Solar system’s terrestrial planets – whose accretion likely took around 10^8 years to complete (e.g. [Chambers 2004](#); [Righter & O’Brien 2011](#)). Conversely, if the embryos grow sufficiently massive prior to the dissolution of the gaseous component of the circumstellar disk (reaching $\sim 10M_{\oplus}$), they become capable of feeding on the gas in the disk, allowing them to rapidly obtain a gaseous envelope ([Perri & Cameron 1974](#); [Johansen et al. 2007](#)). This process of rapid, runaway growth continues until the planet has opened a gap in the circumstellar disk, after which the growth slows markedly as the planet feeds from the edges of that gap. Such feeding will often be accompanied by the migration of the resulting giant planet – a process which can also be driven by the planet’s interaction with the other embryos and planetesimals surrounding the star.

In the Solar system, such migration is suggested by the sculpting of the Asteroid and Edgeworth-Kuiper belts (e.g. [Gomes 1997](#); [Minton & Malhotra 2009, 2011](#)), and the captured Jovian and Neptunian Trojan populations (e.g. [Morbidelli et al. 2005](#); [Lykawka & Horner 2010](#); [Pirani et al. 2019](#)) – revealing that giant planets can migrate both inward and outward during the latter stages of their formation. The hundreds of giant exoplanets that have been orbiting closer than Jupiter orbits the Sun, have forced a re-evaluation of planet formation theories. This phenomenon can be explained, at least partially, by the observational bias that makes these short-period giant planets much easier to detect. It is considered likely that these giant, close-in planets have migrated from their initial formation location inwards to the vicinity of their host stars during their accretion (e.g. [Alibert et al. 2010](#); [Lin & Papaloizou 1986](#); [Lin et al. 1996](#); [Ward 1997a,b](#); [Tanaka et al. 2002](#); [Alibert et al. 2005a,b](#); [Mordasini et al. 2009a,b](#)), though the formation of close-in gas giant planets in-situ via the core-accretion process could still explain the origin of some of these planets (see e.g., [Batygin et al. 2016](#); [Hasegawa et al. 2019](#)).

Three distinct mechanisms have been proposed to explain the inward migration of giant planets from initially distant orbits to become such “hot Jupiters” (e.g. the review by [Dawson & Johnson 2018](#)). The first is a migration process driven by interactions between a young giant planet and the circumstellar disk, as the planet feeds from that disk ([Goldreich & Tremaine 1980](#); [Lin & Papaloizou 1986](#); [Baruteau et al. 2014](#); [Heller 2019](#)). Torques between the planet and the edges of the gap it has opened in the disk can cause the planet to migrate inwards – a process that either ends when the planet reaches the inner edge of the disk, or when the disk itself is stripped by the youthful star ([Lin et al. 1996](#)). The migration of the planet in this mechanism is smooth, with the orbital eccentricity and inclination of the planet’s orbit (with respect to the disk) remaining essentially zero throughout - leading to hot and warm Jupiters moving on circular orbits that are well aligned with the equatorial plane of their host star ([Bitsch et al. 2013](#)).

The second proposed mechanism invokes dynamical excitation and mutual scattering events between giant planets (e.g. [Rasio & Ford 1996](#); [Weidenschilling & Marzari 1996](#); [Lin & Ida 1997](#); [Ford & Rasio 2008](#)). In such a scenario, two giant planets experience a close encounter (or a series of such encounters) that act to significantly increase the orbital eccentricities of both planets. One planet is flung inwards, eventually reaching an orbit with a very small periape. The other planet is flung outwards, onto a highly eccentric orbit with periape close to the apoapse of the

¹ The NASA Exoplanet Archive, <https://exoplanetarchive.ipac.caltech.edu/>, lists 4,569 confirmed exoplanets as of 2021 Nov 15.

² For a detailed overview of our knowledge of the Solar system in the context of exoplanetary science, we direct the interested reader to [Horner et al. \(2020a\)](#), and references therein

inner planet’s orbit. Tidal forces between the star and the inner planet then act to circularise that planet’s orbit at periapsis, decoupling the two planets, and leaving a hot Jupiter on a near circular orbit and a (much) more distant planet with an eccentric orbit (e.g., Nagasawa et al. 2008). In extreme cases, this process could even lead to the ejection of the outer planet from the system entirely. The hot Jupiter so produced would be expected to have low or moderate orbital inclination (relative to the equatorial plane of its star), due to the near-coplanarity expected of the initial orbits of the interacting planets.

The final mechanism involves the dynamical interaction of a massive planet and a distant companion on an orbit inclined by $\gtrsim 30^\circ$ with respect to the plane of the planet’s orbit (Kozai 1962; Lidov 1962). Over timescales much longer than the inner companion’s orbital period, the planet’s orbit is perturbed by the distant companion through a series of Kozai-Lidov oscillations, resulting in the coupled evolution of orbital inclination and eccentricity. Such evolution can drive the planet onto a highly eccentric orbit – at which point tidal interactions between the planet and star at periapsis once again act to circularise its orbit, freezing in the enhanced orbital inclination present at that phase in its cyclical evolution. Hot Jupiters produced in this manner would be expected to display strong orbital misalignment - moving on orbits that are highly tilted, or even retrograde, with respect to the equatorial planes of their host stars (e.g. Fabrycky & Winn 2009; Winn et al. 2009; Naoz et al. 2011; Dalal et al. 2019).

In this context, the study of exoplanetary systems containing hot Jupiters is particularly interesting. It is likely that each of the proposed mechanisms will contribute to the overall population of observed hot Jupiters – and it is interesting to attempt to disentangle which such planets reached their current orbits as a result of which mechanism.

In this work, we examine the HD 83443 planetary system which has long been known to host a hot Jupiter with an orbital period of 2.9855 ± 0.0004 d and an eccentricity of 0.05 ± 0.05 (Butler et al. 2002). A recent re-analysis of the complete California Planet Search catalog by Rosenthal et al. (2021) presented refined parameters of $m \sin i = 0.409 \pm 0.019 M_J$ and $e = 0.074^{+0.031}_{-0.032}$. HD 83443 was reported to host two giant planets in the early days of extrasolar planet search (Mayor et al. 2004), with CORALIE data suggesting a candidate second Saturn-mass planet at an orbital period of 29.8 days. Further independent analysis of Keck/HIRES and AAT/UCLES data by Butler et al. (2002) confirmed the hot Jupiter but found no evidence for a second planet.

Given the lengthy archive of radial velocity data now available for HD 83443, the system stands as an interesting test case for the various theories of planetary migration. If that migration were the result of tidal interaction with the circumstellar disk, it might be the case that additional giant planets orbit at greater distances, awaiting discovery once sufficient data are available. Equally, if the planet were scattered inwards through encounters with another giant planet, then that planet might remain in the system, moving on a highly eccentric orbit – a smoking gun for the origin of the hot Jupiter HD 83443 b.

In this paper, we report the discovery of HD 83443c, a rare highly eccentric long-period giant planet orbiting a star with a known hot Jupiter. Section 2 details the observational data, and in Section 3, we describe the properties of the host star. Section 4 gives the results of the radial-velocity fitting, a dynamical investigation of the HD 83443 system is given in Section 5, and Sections 6 and 7 present our discussion and conclusions.

2. OBSERVATIONS AND DATA REDUCTION

HD 83443 has been observed by four precise radial velocity instruments spanning a baseline of over 22 years. Here we give details about the observations from each instrument. All radial velocities used in this analysis are given in Table 1.

2.1. AAT

The Anglo-Australian Planet Search (AAPS) survey started in 1998. The survey was carried out using the 3.9 m Anglo-Australian Telescope (AAT) and the University College London Echelle Spectrograph (UCLES) with a limiting Doppler precision of 3 ms^{-1} (Tinney et al. 2001). AAPS obtained 25 observations of HD 83443 between UT 1999 Feb 2 and UT 2015 Mar 13.

2.2. HARPS

HARPS is a highly-stabilised spectrometer which began operations in 2003 (Mayor et al. 2003). The HARPS fibre feed was upgraded in 2015 (Lo Curto et al. 2015); here we use 45 observations taken prior to this correction, from UT 2003 Dec 28 to 2015 May 1, and 11 observations that were obtained afterward, from 2015 Dec 10 to 2016 May 28. We use the HARPS radial velocities from Trifonov et al. (2020), which corrected for nightly zero point and CCD stitching offsets.

Table 1. Radial Velocities for HD 83443

Time	Velocity	Uncertainty	Instrument
[BJD]	[m s^{-1}]	[m s^{-1}]	
MINERVA-Australis - ThAr			
2458523.05882338	28316.1248	8.88	MINERVA-ThAr
2458523.06634676	28292.2683	7.54	MINERVA-ThAr
2458527.22736930	28176.2535	10.04	MINERVA-ThAr
2458527.23836497	28196.2810	7.24	MINERVA-ThAr
2458530.13194543	28196.9606	7.77	MINERVA-ThAr
2458530.14292949	28216.8482	9.29	MINERVA-ThAr
2458532.19110159	28248.3593	7.11	MINERVA-ThAr
2458532.20209720	28263.8133	10.75	MINERVA-ThAr
2458533.20590349	28219.9088	13.91	MINERVA-ThAr
2458534.13895505	28283.3215	7.60	MINERVA-ThAr

NOTE—Table 1 is published in its entirety in machine-readable format online. A portion is shown here for guidance regarding its form and content.

2.3. Keck/HIRES

The Keck/HIRES Radial Velocity Survey started in 1994, and focused on the search for exoplanets around low activity F, G, K and M-dwarf stars. This program acquired more than 60,000 radial velocity measurements of 1,624 stars (Butler et al. 2017). A revised data release, correcting for small zero-point offsets and other systematics, was published in Tal-Or et al. (2019). From this database we obtain 45 observations of HD 83443, taken between UT 2000 Dec 19 and 2014 Dec 11.

2.4. MINERVA-Australis

MINERVA-Australis saw first light in 2019, and is a dedicated facility that spends every clear night obtaining radial velocity measurements of stars thought to be potential planet hosts (Wittenmyer et al. 2018; Addison et al. 2019, 2021). MINERVA-Australis consists of an array of four independently operated 0.7 m Planewave CDK700 telescopes situated at the Mount Kent Observatory in Queensland, Australia (Addison et al. 2019). Each telescope simultaneously feeds stellar light via fibre optic cables to a single KiwiSpec R4-100 high-resolution ($R = 80,000$) spectrograph (Barnes et al. 2012) with wavelength coverage from 480 to 620 nm.

A total of 22 individual spectra for HD 83443 were obtained between 2019 Feb 8 and 2021 Feb 22 using MINERVA-Australis telescope 4. Of these, 17 epochs used the simultaneous Th-Ar calibration fibre, and 5 epochs used a simultaneous back-illuminated iodine cell for wavelength calibration. The latter technique was employed from 2019 Dec 4 to mitigate the loss of spectral information due to saturation from the argon lines. Radial velocities were derived by cross-correlation, where the template being matched is the mean spectrum.

3. STELLAR PROPERTIES OF HD83443

Table 2 summarises the literature measurements for the properties of HD 83443. HD 83443 is a solar mass K0 star, with more than twice the metallicity of the Sun. This enhanced metallicity is consistent the well-established giant planet-metallicity correlation (e.g. Fischer & Valenti 2005; Jones et al. 2016; Wittenmyer et al. 2017a; Ghezzi et al. 2018; Osborn & Bayliss 2020; Fulton et al. 2021). For the orbit fitting and derivation of planetary parameters, we adopt a stellar mass of $1.00 \pm 0.03 M_{\odot}$ (Delgado Mena et al. 2019).

4. ORBIT FITTING AND RESULTS

While HD 83443 was part of the main Anglo-Australian Planet Search for 16 years (Wittenmyer et al. 2020), the sparse sampling prevented the detection of longer-period radial velocity signatures. Inspection of additional publicly available data (CORALIE, HARPS, HIRES) with the Geneva group’s DACE tool³ revealed evidence for a potential

³ <https://dace.unige.ch/dashboard/>

Table 2. Stellar parameters for HD 83443. The adopted stellar mass is indicated in bold.

Parameter	Value	Reference
Right Ascension (h:m:s)	9:37:11.8276	1
Declination (d:m:s)	-43:16:19.9326	1
Distance (pc)	40.95 ± 0.06	2
Spectral type	K0 V	3
$(B - V)$	0.811	4
T_{eff} (K)	5429^{+96}_{-122}	5
	5487^{+90}_{-107}	6
	5442 ± 17	7
$\log g$ (cm^2/s)	$4.41^{+0.08}_{-0.07}$	5
	4.39 ± 0.04	7
	4.43 ± 0.08	8
R_* (R_{\odot})	$1.005^{+0.055}_{-0.038}$	5
	$0.982^{+0.039}_{-0.031}$	6
	0.94 ± 0.02	7
L_* (L_{\odot})	$0.790^{+0.020}_{-0.015}$	5
	0.787 ± 0.002	6
	$0.72^{+0.12}_{-0.10}$	9
M_* (M_{\odot})	0.95 ± 0.12	5
	0.79 ± 0.07	7
	1.05 ± 0.10	9
	1.00 ± 0.03	12
Metallicity, [Fe/H]	0.34 ± 0.03	8
	0.44 ± 0.04	9
	0.35 ± 0.08	11
Age (Gyr)	3.2	4
	2.64 ± 2.49	12
ρ_* (g cm^{-3})	1.32 ± 0.28	5
$v \sin i$ (km s^{-1})	1.4	4
	1.3 ± 0.5	10
P_{rot} (day)	35.3	4

References—1. Gaia Collaboration et al. (2018); 2. Gaia Collaboration (2018); 3. Houk (1978), 4. Mayor et al. (2004), 5. Stassun et al. (2019), 6. Gaia Collaboration et al. (2018), 7. Stassun et al. (2017), 8. Sousa et al. (2008), 9. Ghezzi et al. (2010), 10. Valenti & Fischer (2005), 11. Santos et al. (2004), 12. Delgado Mena et al. (2019)

high-eccentricity, long-period signal. We then performed some initial simple analysis with *Systemic Console 2.200* on the Keck/HIRES, HARPS and AAT data sets (see Section 2). Those initial efforts supported the existence of a highly eccentric planet with a period of ~ 6800 or ~ 10000 days.

For the final fitting, we performed two runs with *Exostriker* (Trifonov 2019), with initial values for the period of the outer planet at 6000 days and 10000 days. All other priors and starting values were identical between the two runs (Table 3). The radial velocity time series, the phase-folded plot for the inner planet and the linear time plot for the outer one can be seen in figure 1.

We explore the parameter space running a Markov Chain Monte Carlo sampling of the posterior solutions using *emcee* (Foreman-Mackey et al. 2013) with 88 walkers and 5000 steps. Corner plots for both runs can be seen in the Appendix A; the posteriors are unimodal and consistent with a highly significant and unique solution. Posteriors and results are included in Table 3. Some statistical values related to both runs with *Exostriker* are included in table 4. Both *Exostriker* runs converged on essentially identical solutions. The results support the presence of a long-period, highly eccentric outer planet. The critical periastron velocity excursion is sampled independently by HARPS and Keck/HIRES, giving further support to the interpretation as Keplerian orbital motion.

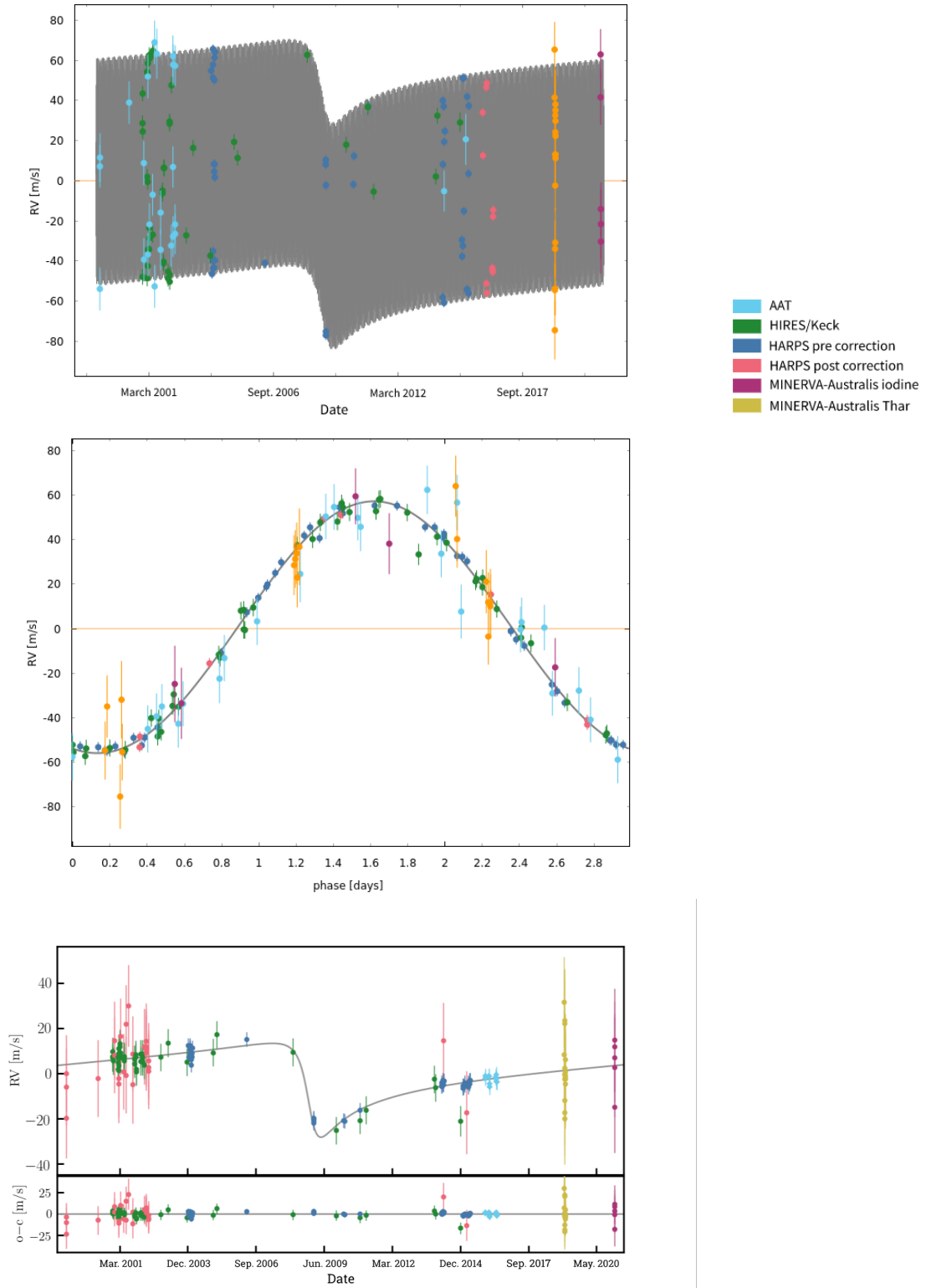


Figure 1. The observational data for HD 83443, colour coded as follows: Light blue - AAT (Tinney et al. 2001), Green - HIRES/Keck (Tal-Or et al. 2019), Blue - HARPS pre-correction (Trifonov et al. 2020), Red - HARPS post correction (Trifonov et al. 2020), Orange - MINERVA-Australis ThAr (Addison et al. 2019) and Purple - MINERVA-Australis iodine (Addison et al. 2019). The top panel shows all the data as a function of time, with the two planet solution shown in black. The centre panel shows the data phase folded for HD 83443 b only (centre panel), with the lower panel showing the data for the long period planet, HD 83443 c (lower panel).

Table 3. MCMC sampling posteriors and priors of the orbital and nuisance parameters of the HD 83443 system, derived by radial velocities (MINERVA, AAT, HARPS, HIRES/Keck). Derived jitter values are simply added in quadrature to the reported error bars.

Parameter	Median and 1σ	Adopted priors
K_b [m s^{-1}]	$56.73^{+0.36}_{-0.36}$	$\mathcal{U}(0, 10^4)$
P_b [day]	$2.985628^{+0.000005}_{-0.000005}$	$\mathcal{U}(0, 10^5)$
e_b	$0.012^{+0.007}_{-0.006}$	$\mathcal{U}(0,1)$
ω_b [deg]	344^{+11}_{-15}	$\mathcal{U}(0,360)$
$M_{0,b}$ [deg]	335^{+15}_{-11}	$\mathcal{U}(0,360)$
a_b [au]	0.0406 ± 0.0004	(derived)
$m \sin i_b$ [M_{jup}]	0.402 ± 0.008	(derived)
K_c [m s^{-1}]	$20.7^{+2.2}_{-1.6}$	$\mathcal{U}(0, 10^4)$
P_c [day]	8241^{+1019}_{-530}	$\mathcal{U}(0, 10^5)$
e_c	$0.760^{+0.046}_{-0.047}$	$\mathcal{U}(0,1)$
ω_c [deg]	$118.2^{+5.6}_{-5.7}$	$\mathcal{U}(0,360)$
$M_{0,c}$ [deg]	$281.0^{+7.9}_{-4.9}$	$\mathcal{U}(0,360)$
a_c [au]	8.0 ± 0.8	(derived)
$m \sin i_c$ [M_{jup}]	$1.35^{+0.07}_{-0.06}$	(derived)
RV off. _{HARPSpre-correction} [m s^{-1}]	$-0.8^{+0.5}_{-0.5}$	$\mathcal{U}(-10^5, 10^5)$
RV off. _{HARPSpost-correction} [m s^{-1}]	$4.9^{+0.9}_{-1.0}$	$\mathcal{U}(-10^5, 10^5)$
RV off. _{HIRES/Keck} [m s^{-1}]	$-5.7^{+0.6}_{-0.6}$	$\mathcal{U}(-10^5, 10^5)$
RV off. _{AAT} [m s^{-1}]	$9.0^{+2.2}_{-2.2}$	$\mathcal{U}(-10^5, 10^5)$
RV off. _{MINERVA-Australisiodine} [m s^{-1}]	$28205.9^{+7.2}_{-7.2}$	$\mathcal{U}(-10^5, 10^5)$
RV off. _{MINERVA-AustralisThAr} [m s^{-1}]	$28250.8^{+3.5}_{-3.4}$	$\mathcal{U}(-10^5, 10^5)$
RV jitter _{HARPSpre-correction} [m s^{-1}]	$1.9^{+0.3}_{-0.3}$	$\mathcal{U}(0, 10^4)$
RV jitter _{HARPSpost-correction} [m s^{-1}]	$1.9^{+0.7}_{-0.5}$	$\mathcal{U}(0, 10^4)$
RV jitter _{HIRES/Keck} [m s^{-1}]	$3.5^{+0.6}_{-0.5}$	$\mathcal{U}(0, 10^4)$
RV jitter _{AAT} [m s^{-1}]	$9.8^{+2.2}_{-1.7}$	$\mathcal{U}(0, 10^4)$
RV jitter _{MINERVA-Australisiodine} [m s^{-1}]	$10.2^{+10.9}_{-6.3}$	$\mathcal{U}(0, 10^4)$
RV jitter _{MINERVA-AustralisThAr} [m s^{-1}]	$10.3^{+4.1}_{-3.5}$	$\mathcal{U}(0, 10^4)$

NOTE— $\mathcal{U}(l,u)$ signifies a uniform prior with lower bound l and upper bound u .

NOTE—Mean anomalies M_0 are for epoch BJD 2453001.85.

5. DYNAMICAL SIMULATIONS AND LIMITS ON ADDITIONAL PLANETS

The two planets described orbiting HD 83443 in this work are sufficiently widely separated to be effectively dynamically decoupled from one another. As such, it seems likely that there is a vast amount of space in the system that could host additional planets – so long as such planets were not disrupted or ejected by whatever process led to the highly eccentric orbit of HD 83443 c, and the inward migration of HD 83443 b.

5.1. The Dynamical Stability of the HD 83443 Planetary System

Table 4. Statistical values for *Exostriker* runs.

Period (days)	Ecc	Chi	RMS	WRMS	lnL	BIC	AIC	Initial period (days)
8240	0.7598	1.0442	7.01	3.91	-418.07	946.08	792.14	6000
8203	0.7590	1.0923	7.03	3.93	-419.72	949.38	795.45	10000

In order to explore this possibility, we performed a suite of n -body simulations, using the Hybrid integrator within the MERCURY integration package [Chambers \(1999\)](#). We use a similar methodology to that laid out in [Horner et al. \(2022\)](#), distributing a large population of massless test particles between the orbits of the two planets, and following their dynamical evolution for a period of one million years. Due to the small orbital distance of HD 83443 b and the test particles used in the inner regions of the system, a purely Newtonian approach to the dynamical simulations would be inappropriate. We therefore used a version of MERCURY modified to include the first-order post-Newtonian relativistic corrections, as described in [Horner et al. \(2020b\)](#), following [Gilmore & Ross \(2008\)](#). Test particles were removed from the simulations upon colliding with either of the planets in the system, the central object, or upon reaching a distance of 20 au from the system barycentre (and hence having been transferred to a chaotic orbit crossing that of HD 83443 c). The simulation timestep was 0.08 days, and the entire suite of simulations took approximately six months to run, distributed across the nodes of USQ’s *Fawkes* supercomputing cluster - equivalent to approximately 250 years of CPU time.

Test particles were distributed in a regular grid in $\log a - e - \omega - M$ space, with the initial orbital inclinations of both the planets and the test particles set to zero⁴. In total, 13.6 million test particles were created. 492 unique values of semi-major axis were used as initial conditions for those test particles, evenly distributed in $\log a$ space between 0.04095765 and 8.04146231 au. At each of those 492 unique semi-major axes, 123 unique orbital eccentricities were used, evenly distributed in the range 0.0 to 0.9. At each of these 60516 $a - e$ pairs, 45 unique values of ω were chosen, evenly distributed between 0 and 360°. Finally, at each of these 2723220 $a - e - \omega$ locations, 5 unique values of mean anomaly were tested - again evenly distributed between 0 and 360°. The orbits and masses of the two planets were taken directly from Table 3, and are therefore the minimum feasible masses for the planets based on the radial velocity observations. Since the simulations assume the system to initially be coplanar, this seems a reasonable assumption to make.

Of the 13.6 million test particles whose orbital evolution was followed in our simulations, just over 7.9 million were removed from the system within the 1 Myr of our integrations, with particles colliding with one or other of the two planets (~ 2.8 million), falling into the central star (~ 430000) or being ejected beyond a barycentric distance of 20 au (~ 4.7 million). The time at which each of those ~ 7.9 million test particles was removed from the system was recorded, and the results used to generate the stability plots shown in Figure 2. In each of the two panels in that figure the lifetime shown at a given $a-e$ location is the mean of the ejection times across the 225 test particles that began the simulation at that particular $a-e$ location.

It is immediately apparent from Figure 2 that the vast majority of the 5.7 million test particles that survived the full 1 Myr duration of the simulations were located interior to ~ 1.2 au, forming a broad island of stability bounded, at the inner edge, by orbits that approach HD 83443 b (i.e. periastra of ~ 0.05 au), and at the outer edge, by orbits with apastras of ~ 1.2 au⁵. The left hand panel of Figure 2 plots semi-major axes logarithmically, which allows fine structures in the inner region to be clearly seen. In that inner ‘unstable wedge’, carved by HD 83443 b, there are a large number of narrow strips of stability rising to large eccentricities, at the locations of mean-motion resonances between test particles and HD 83443 b.

Perhaps the most pronounced of these resonant features falls right at the inner edge of the plot, with a large number of stable test particles trapped in 1:1 mean-motion resonance with the innermost planet. Such particles are analogues of the Solar system’s Jovian and Neptunian Trojan populations (see e.g. [Levison et al. \(1997\)](#); [Jewitt et al. \(2000\)](#);

⁴ In other words, the system was modelled under an implicit assumption of initial coplanarity, on the grounds that no information was available on the mutual inclination of the two known planets.

⁵ It should be noted, here, that just because a region would be stable for a particle of minimal or zero mass, that will remain true for objects of arbitrarily large mass. Clearly, at any given location, there is a maximum mass for which such an orbit would remain stable. However, our simulations nonetheless serve as a good guide to the regions of the system that are definitely unstable, from the point of view of additional companions.

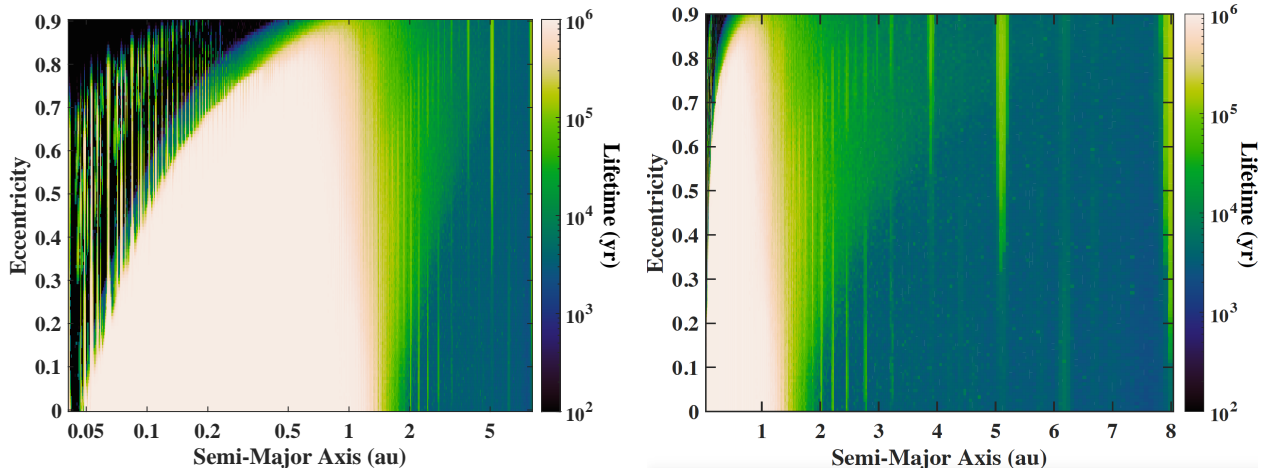


Figure 2. The dynamical stability of massless test particles in the HD 83443 system, as a function of their initial semi-major axis and eccentricity, from simulations spanning a period of 1 Myr. The stability of the inner region of the system is dominated by the influence of HD 83443 b, with test particles that approach that planet too closely being removed from the system on short timescales. In the outer regions of the system, stability is strongly influenced by HD 83443 c, which renders most orbits beyond ~ 1.5 au unstable due to its high eccentricity (reaching a periastron distance of 1.92 au). We note that, since the simulations covered a period of 1 Myr, the regions in white are those where test particles have minimum lifetimes of 1 Myr. It is highly likely that, across much of that space, lifetimes would be far longer than the 1 Myr of our simulations.

Horner & Lykawka (2010); Holt et al. (2021), and Horner et al. (2020a) for a more general overview) - populations of asteroids trapped in the same mean-motion resonance, moving on stable orbits that librate around the leading and trailing Lagrange points (L_4 and L_5) in the orbits of the giant planets. In the Solar system, the populations of stable Trojan companions to the giant planets are thought to have been captured during the final stages of planetary migration (e.g. Morbidelli et al. 2005; Lykawka & Horner 2010; Nesvorný et al. 2013) - and the presence of those stable Trojan test particles in our runs serves as a reminder that there is the possibility that the inward migration of giant planets could lead to the capture and transport of Trojans in exoplanetary system (as discussed in e.g. Érdi & Sándor 2005; Schwarz et al. 2007; Madhusudhan & Winn 2009; Tinney et al. 2011; Leleu et al. 2019).

The large number of narrow resonant strips of stability found in this region is the direct result of the high density of test particles deployed in these runs - sampling the space in the inner wedge with sufficient precision that we capture as many resonant features as possible - rather than having test particles distributed such that they can skip resonant orbits at the time of creation. Whilst such oversampling might seem excessive, the presence of so many potentially stable resonant scenarios (particularly those where the stable feature extends down to circular orbits) fits well with the discovery of a number of tightly dynamically packed exoplanetary systems in recent years (e.g. Luger et al. 2017; Shallue & Vanderburg 2018; Lam et al. 2020; Leleu et al. 2021).

Since HD 83443 c is not known to transit the disk of its host star, its orbital inclination remains unconstrained. As such, it is interesting to consider what impact an inclined orbit for HD 83443 c might have on the stability of the rest of the planetary system. To investigate this, we therefore carried out five ancillary sets of simulations, to consider the impact of the inclination of the orbit of HD 83443 c relative to that of the inner planet and disk of test particles. Those simulations used identical suites of test particles, again distributed between the orbits of the two planets. The initial orbits of those test particles were co-planar with the orbit of HD 83443 b. In total, we simulated the evolution of 686,340 test particles in each scenario. The evolution of those test particles was again followed for a period of one million years, or until they collided with one of the system’s massive objects, or were ejected. From one simulation to the next, the only changes we made to the initial conditions were to increase the orbital inclination of HD 83443 c, testing inclinations of 5, 15, 30, 45, and 60 degrees to the orbit of the innermost planet and test particle disk (in a manner similar to that used in e.g. Horner et al. (2011) and Horner et al. (2013)). For each orbital inclination, we recalculated the mass of HD 83443 c, increasing it such that the $M \sin i$ value of that mass was held constant. As the inclination of the planet’s orbit increased, therefore, so did the mass of the planet in our simulations.

The results of these simulations are shown in Figure 3. As the inclination of HD 83443 c is increased, the outer boundary of the stable region (which, in the main runs, was located at ~ 1.2 au) slowly moves to smaller semi-major

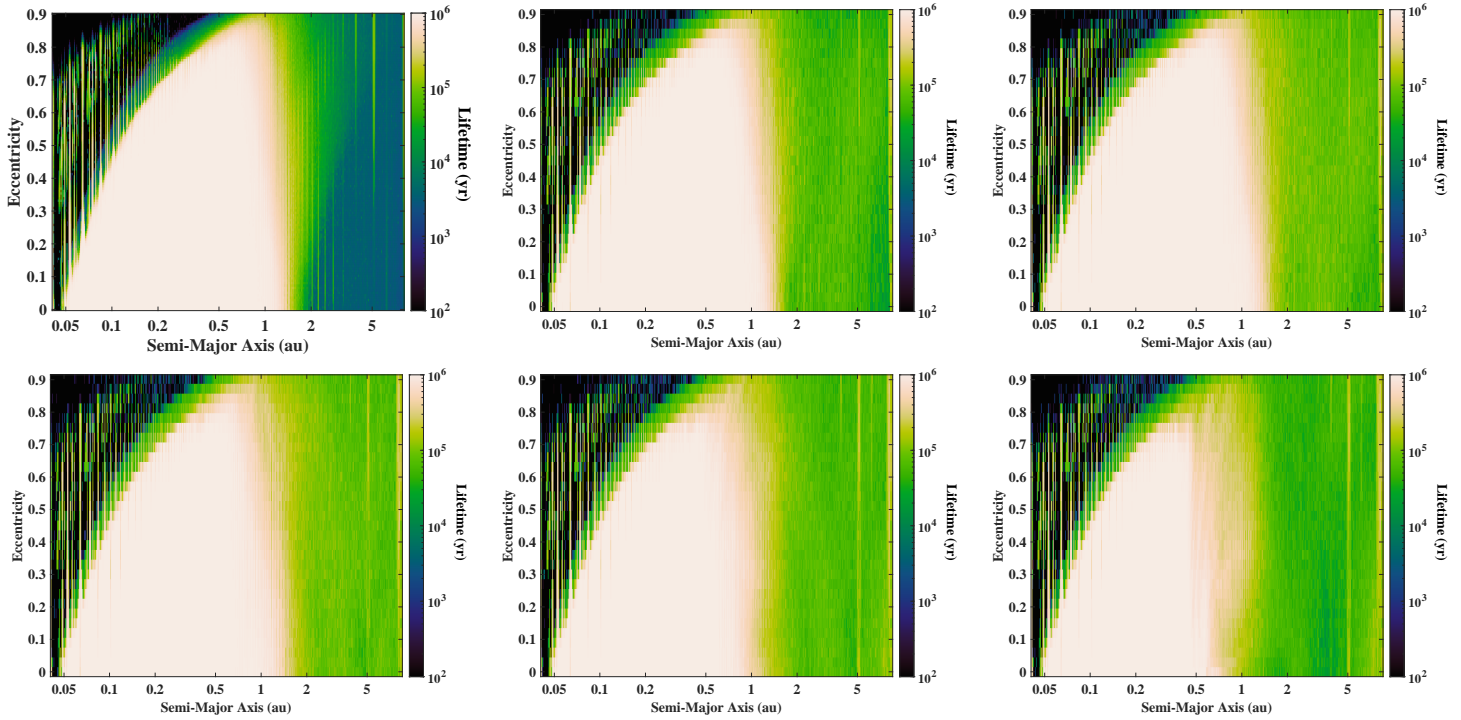


Figure 3. The dynamical stability of massless test particles in the HD 83443 system, for simulations considering a variety of orbital inclinations for the orbit of HD 83443c. The top left hand panel shows the case where the system begins in a fully co-planar state, with HD 83443c moving on an orbit that is in the same plane as the disk of test particles and the orbit of HD 83443b, as presented in Figure 2. The remaining panels feature simulations at lower resolution, following the evolution of 686,340 massless test particles. The central plot of the top row shows the outcome with HD 83443c moving on an orbit tilted by 5 degrees to the disk and inner planet; top right has c on an orbit inclined by 15 degrees; lower left has an inclination of 30 degrees; lower centre has an inclination of 45 degrees, and lower right, 60 degrees. As with Figure 2, the simulations spanned a period of 1 Myr. Again, since the simulations covered a period of 1 Myr, the regions in white are those where test particles have minimum lifetimes of 1 Myr. It is highly likely that, across much of that space, lifetimes would be far longer than the 1 Myr of our simulations. Moderate levels of mutual inclination between the orbits of the outer planet and the disk do little to alter the stability profile, but once the orbit of HD 83443c is inclined by 45 and 60 degrees, it begins to whittle away at the outer edge of the stable area, rendering orbits in the region beyond ~ 0.9 au (45 degree) and ~ 0.5 au (60 degree) unstable on timescales of hundreds of thousands of years.

axes. This effect is most pronounced for the two most inclined simulation sets - with the outer planet inclined by 45 and 60 degrees. As the mass of HD 83443c is increased between runs, the breadth of the unstable region also increases. For the coplanar scenario, the outer edge of the stable region is located at ~ 1.2 au, which is 5 Hill radii interior to the location of the planet at periastron. At an inclination of 60 degrees, the mass has only doubled. Since the Hill radius of a planet is proportional to the cube root of the planet's mass, this doubling in mass only increases the size of that planet's Hill sphere by approximately 26%. At periastron, this corresponds to shifting the outer edge of the stable region to ~ 1 au. In actuality, our simulations show that the unstable region for the 45 degree and 60 degree simulations stretches farther inward than would be expected based solely on the width of HD 83443c's Hill sphere. This is the direct result of the increased inclination of the outer planet, which acts to drive the orbital eccentricity and inclination of test particles in the outer region of the disk to vary, driving the apastras of those test particles to locations within the dynamical sway of the giant planet. Despite this, there remains a large region in the inner parts of the HD 83443c system that is dynamically stable on million year timescales, offering significant scope for the existence of additional, as yet undetected, planets.

5.2. Could additional planets lurk in the stable area of the system?

Having determined the regions in which additional planets are dynamically permitted, we ran injection-recovery simulations to set upper mass limits on the planets that can be ruled out by the radial velocity data (e.g. [Wittenmyer et al. 2006, 2009](#); [Fulton et al. 2021](#)). For this analysis, we used *RVSearch* ([Rosenthal et al. 2021](#)) to generate 3000 fictitious planets over a wide range of masses and orbital separations. The results are shown in Figure 4 as a detectability map. In the dynamically stable region interior to approximately 1 au, the radial velocity data rule out the presence of planets more massive than $10\text{-}40 M_{\oplus}$, but smaller, potentially rocky planets may yet lurk undetected in this region (e.g. Section 6.3).

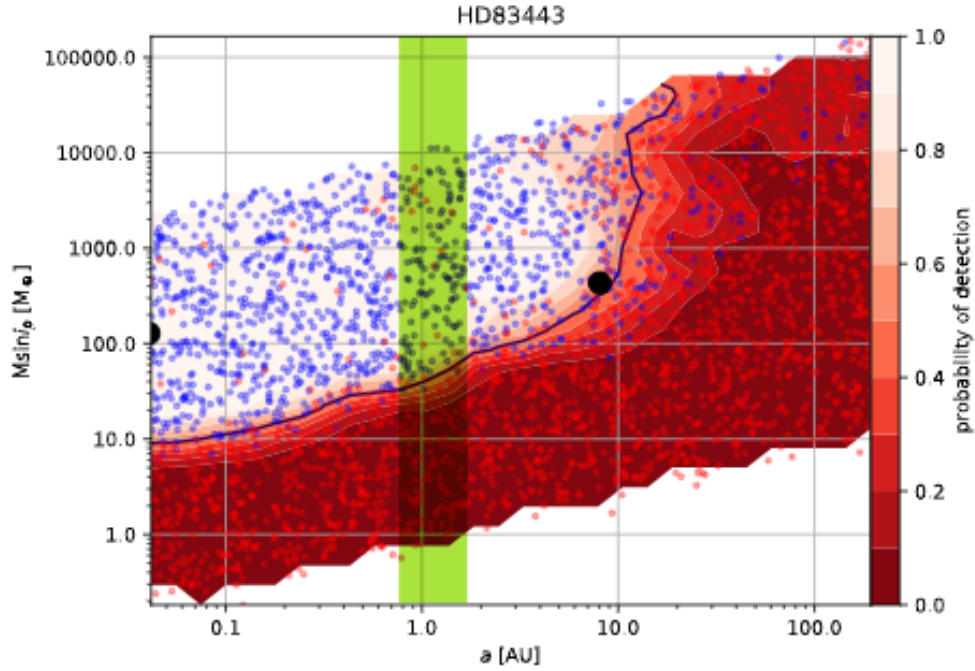


Figure 4. *RVSearch* results for detectability of additional planets in the HD 83443 system. HD 83443b and c are shown as large black points, and the injected test planets are shown as small blue points. The solid black line indicates a 50% detection probability. HD 83443c lies within the region of high detectability, and the radial velocity data can exclude additional planets larger than $\sim 10\text{-}40 M_{\oplus}$ interior to 1 au, the region shown to be dynamically stable. The optimistic habitable zone is shaded in green.

6. DISCUSSION

6.1. Searching for transits of the inner planet

If HD 83443 b transits, it is expected to have been observed by *TESS* given the short orbital period of the b planet (~ 3 days) relative to the baseline of each continuous segment of *TESS* observations (~ 13 day spacecraft orbit). Phase modulations may also be observed for HD 83443 b given its short orbital period and the continuous orbital phase coverage by *TESS*. The expected semi-amplitudes of the modulations caused by Doppler boosting and ellipsoidal variations are expected to be < 1 ppm, which is below our detection limit for the *TESS* photometry. The semi-amplitude caused by atmospheric reflection and thermal emission of the planet is dependent on the planet’s albedo and temperature, but could be as high as ~ 150 ppm for a perfectly reflective (1.0 geometric albedo) planet.

The *TESS* spacecraft obtained time-series photometry of HD 83443 at 2-min cadence initially during Sector 9 observations (UT 2019 Feb 28 through 2019 Mar 25), and again nearly two years later during Sectors 35 and 36 (UT 2021 Feb 09 through 2021 Apr 02). The light curves are publicly available on the Mikulski Archive for Space Telescopes⁶ (MAST) and include the simple aperture photometry (SAP) and the pre-search data conditioning (PDC) light curves that were processed by the Science Processing Operations Center (SPOC) pipeline (Jenkins et al. 2016). We searched for evidence of transit events and phase modulations caused by the inner planet in the *TESS* photometry using the orbital period and time of conjunction from the radial velocity analysis ($T_c = 2455000.3216_{-0.0076}^{+0.0068}$ BJD). The PDC light curves from each individual *TESS* sector and the concatenated light curve were folded in phase to the period of the b planet such that the anticipated transit of HD 83443 b would occur at 0 phase, and are shown in Figure 5. The PDC photometry exhibits modulations up to 100 ppm, but the observed maxima and minima of the modulations may be consistent with the timings of thruster firings by the *TESS* spacecraft (blue triangles). The thrusters are used to periodically (every ~ 2 –3 days) stabilize the spacecraft during observations (i.e., momentum dumps), but these events can cause systematic periodicities in the extracted light curves. Figure 5 also shows an example of the anticipated phase curve that could be observed, with modulations of ~ 50 ppm, if HD 83443 b had a 0.3 albedo. However, hot Jupiters with observable phase curves typically exhibit albedo measurements that are nearly zero (e.g., Wong et al. 2020, 2021; Kane et al. 2020). Overall, the observed phase curve of HD 83443 b differs between individual *TESS* sectors, has a shape that is inconsistent with either a transit event or possible emission/reflection modulations by the planet, and is consistent with being flat in the concatenated *TESS* light curve up to 20 ppm. Therefore, we rule out transits and phase modulations of the inner planet, HD 83443 b.

6.2. Dynamical mass of HD 83443c from Astrometry

We have used *Gaia* and *Hipparcos* long-baseline proper motion anomalies from the eDR3 version of the *Hipparcos-Gaia* Catalog of Accelerations (HGCA; Brandt 2018, 2021) to break the $\sin i$ degeneracy and measure the dynamical mass of HD 83443c. HD 83443 is not accelerating in the eDR3 version of the HGCA (its astrometric χ^2 is only 0.15), indicating that a single-star solution fits the observed sky path extremely well. However, due to the excellent precision for HD 83443 in *Gaia* eDR3 (RUWE=0.939), HD 83443c should have induced a detectable astrometric proper motion anomaly at nearly all masses above its radial velocity minimum mass. This means that although HD 83443 is not an astrometric accelerator, we can exclude a vast range of masses above the radial velocity minimum mass and arrive at a strong dynamical mass constraint. This firmly places HD 83443c into the planetary regime.

We estimate the astrometric mass of HD 83443c using the same methods as Brandt et al. (2021a) and Dupuy et al. (2021). We first compute an astrometric mass posterior. We draw five thousand trial orbits for HD 83443c, adopting as priors all the posteriors on the fitted elements from the radial velocity analysis. We adopt a uniform prior on Ω and a geometric ($\sin i$) prior on the inclination i , because these two elements are not constrained by the radial velocities. We use a Gaussian prior on the stellar mass of $1.00 \pm 0.03 M_\odot$, identical to the measurement by Delgado Mena et al. (2019).

For each trial orbit, we solve for the best fit mass and error on that mass (see Section 2 of Brandt et al. 2021a) using *htof* (Brandt et al. 2021b,c) version 1.0.1. We then add the posteriors from each of the 5000 orbital draws to arrive at the astrometric mass posterior for HD 83443c. This mass posterior is shown by the dotted line in Figure 6. The posterior is peaked at zero, an attribute owed to the excellent cross calibration of the HGCA and the fact that

⁶ <https://archive.stsci.edu/>

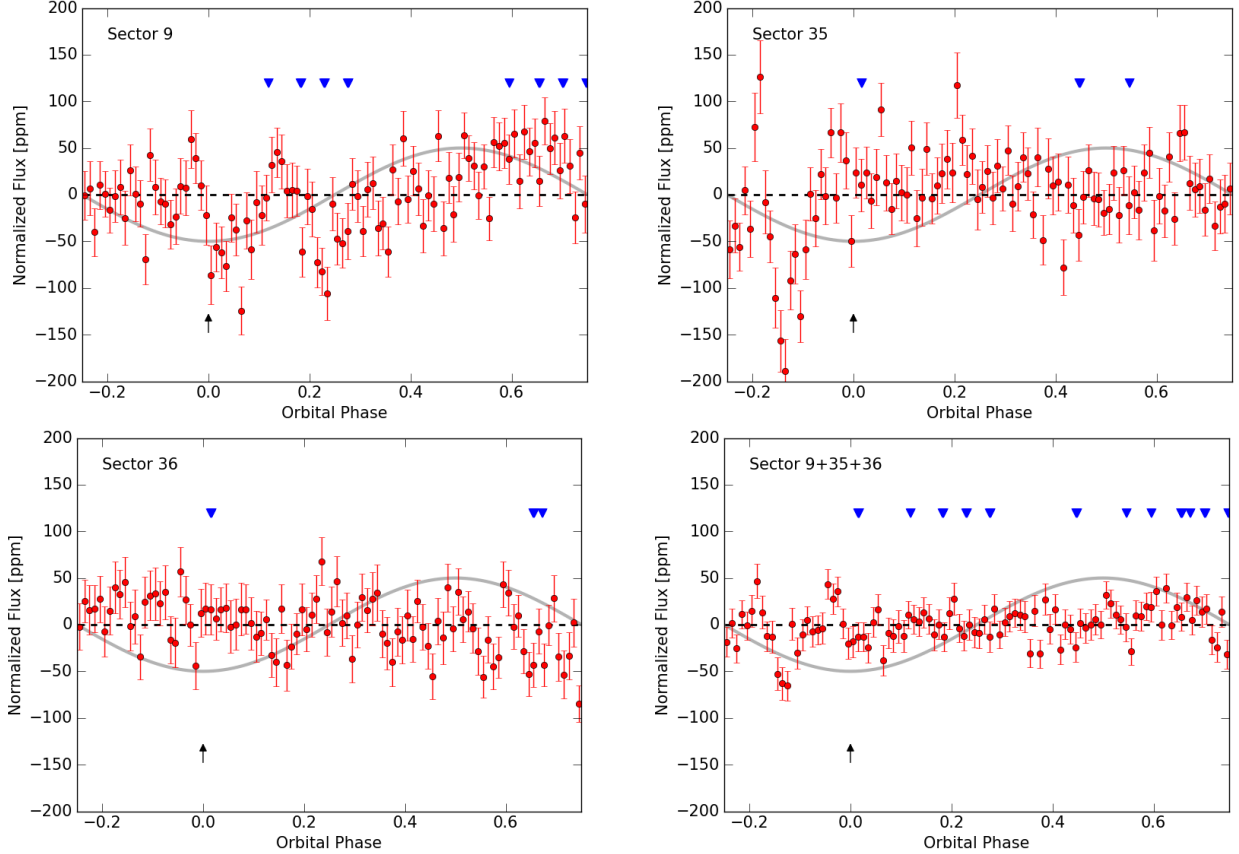


Figure 5. The binned *TESS* PDC light curves phase folded on the orbital period of HD 83443 b (2.985 days) for Sector 9 (top left), Sector 35 (top right), Sector 36 (bottom left), and the concatenated light curve (bottom right). The red points show the binned photometry and their uncertainties show the standard deviation of the individual data points contained within each bin. The individual data points scatter beyond the shown flux limits and, thus, are not shown. The blue triangles indicate spacecraft thruster firing timings (i.e., momentum dumps). The black arrow indicates the expected time of transit at 0 phase and the gray curve shows an example of the expected phase modulations if the planet had 0.3 albedo. The observed modulations are inconsistent between *TESS* sectors and tend to align with momentum dump timings. Therefore, we conclude that we do not observe any evidence for transit events or phase modulations by HD 83443 b.

this source is a non-accelerator. The mass of HD 83443c is constrained to be less than $3.5M_{\text{Jup}}$ with 99.7% confidence from astrometry alone.

Figure 6 shows in red the posterior on the mass from the radial velocity fit. The long tail to high masses is due to the $\sin i$ degeneracy, where high masses are geometrically disfavored. Multiplying the radial velocity mass posterior by the astrometry mass posterior results in the black curve of Figure 6, which is the expected mass posterior that would result from a joint orbital fit to both the radial velocities and proper motion anomaly. Effectively, the final mass posterior is the astrometry mass upper limit (which excludes all masses above $3.5M_{\text{Jup}}$ with 3σ confidence) cut off on the lower end by the radial velocity minimum mass (which allows only masses above $1M_{\text{Jup}}$ with 3σ confidence). The black posterior is our final mass estimate for HD 83443c: $1.5^{+0.5}_{-0.2}M_{\text{Jup}}$ (1σ confidence interval).

We confirm this mass estimate by performing a 3-body joint orbital fit of the radial velocities and astrometry using *orvara* (Brandt et al. 2021d). *orvara* employs MCMC with *ptemcee* (Foreman-Mackey et al. 2013; Vausden et al. 2016). Absolute astrometry is processed and fit for the five astrometric parameters by *htof* at each MCMC step. We use a parallel-tempered MCMC with 20 temperatures; for each temperature we use 100 walkers with 1 million steps, thinned by a factor of 200. We use the standard, uninformative, priors on each of the orbital elements as discussed in Li et al. (2021), except we adopt a uniform prior on planet mass instead of the standard $1/M$ prior. Convergence is assessed by the same criterion as in Li et al. (2021) and Brandt et al. (2021e).

The result of the joint MCMC fit is shown by the grey histogram in Figure 6. The fits to the proper motions are displayed in Figure 7, where higher masses (yellow traces) result in proper motion accelerations that are further and

further disfavored by the data. The MCMC mass posterior agrees nearly perfectly with the product of the radial velocity and astrometry mass posteriors. The derived orbital parameters are consistent with those in Table 3. The inclination posterior is constrained to be $90 \pm 33^\circ$, and the crucial extreme values of inclination ($< 15^\circ$ and $> 165^\circ$) are disfavored by factors of at least e^{20} in likelihood. The mass, separation, and age of HD 83443 c makes it a near-Jupiter analogue.

This mass posterior can be improved over the coming decade with more data; but it is unlikely to improve significantly for the following reasons. First, because HD 83443 is already in the optimal magnitude range for *Gaia* (G mag of 8). The astrometric precision (≈ 0.01 mas in both right-ascension and declination) for HD 83443 is projected to improve by only a small factor by mission-end ⁷. Improvements to the astrometric mass limit could be as great as a factor of two, but likely not greater. Second, the period is 22 years long, and so we need another ~ 10 years of radial velocity to improve noticeably. And third, this mass measurement and the system’s ≈ 5 Gyr age implies a magnitude so faint that we will not obtain direct imaging in thermal emission on this planet soon, even with the James Webb Space Telescope.

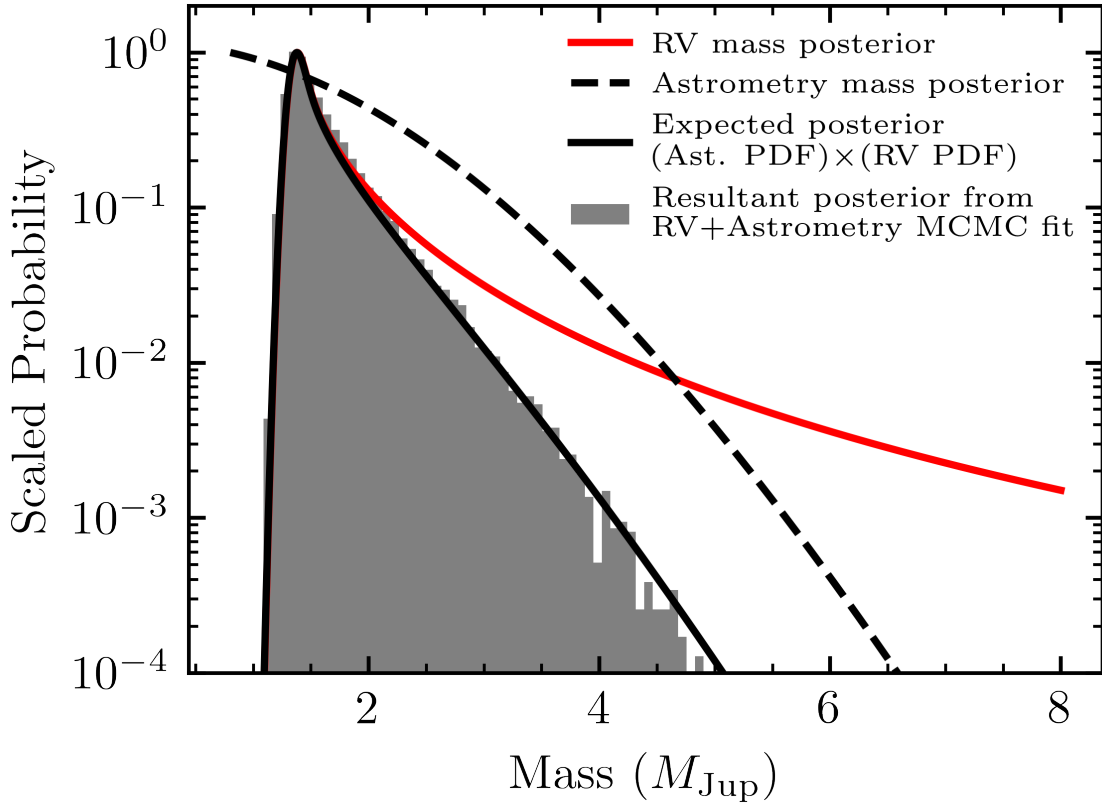


Figure 6. The mass of HD 83443c is the product of a lower limit set by radial velocities and a tight, astrometric upper limit constrained by its lack of acceleration between *Hipparcos* and *Gaia* eDR3. In red is the mass posterior from fitting radial velocities alone (i.e., the Gaussian $m \sin i$ constraint convolved with the $\sin i$ degeneracy). The black dashed line is the mass posterior implied by the lack of astrometric acceleration. The solid black line is the product of the red radial velocity posterior and the dashed-black astrometric posterior. The grey histogram is the resulting mass posterior from a joint orbital fit to the astrometry and radial velocities using *orvara*. The derived mass for HD 83443c is $1.5^{+0.5}_{-0.2} M_{\text{Jup}}$ with 1σ confidence and $1.5^{+2.0}_{-0.3} M_{\text{Jup}}$ with 3σ confidence.

6.3. Direct Imaging Prospects and the Habitable Zone

⁷ <https://www.cosmos.esa.int/web/gaia/sp-figure1>

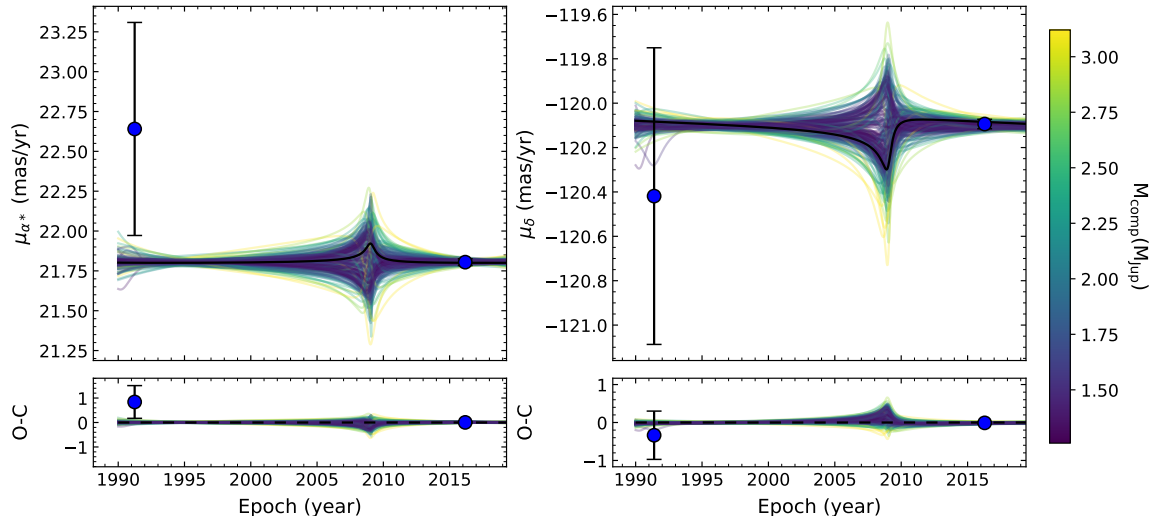


Figure 7. Note to editor: this figure is new. Model proper motions compared to the calibrated *Hipparcos* (point at 1991.25) and *Gaia* EDR3 proper motions (point at 2016) from the HGCA. The best fit orbit is shown in black. A random sampling of other orbits from the MCMC chain are shown and are color coded by the mass of HD 83443 c. Note that the fit to the long-baseline proper motion between *Gaia* and *Hipparcos* is not shown because it is an integral constraint.

An interesting aspect worth exploring for the newly discovered outer planet is its feasibility to be directly imaged by future space-based direct imaging missions thanks to the large angular separation and high eccentricity of its orbit (Kane 2013; Kane et al. 2018). To calculate the brightness of the outer planet, we used the orbit visualization tool described by Li et al. (2021) to carry out a first-order estimation of the planet-to-star flux ratio (i.e., without taking into account noise sources such as background stars and sky noise, exozodiacal dust, residual starlight, detector noise etc.). The flux ratio estimation assumed a Lambert sphere phase function, a planetary radius of $\sim 1.2 R_J$ (estimated from the derived mass at edge-on inclination using a mass-radius relation by Chen & Kipping (2017)), and a geometric albedo of 0.5, consistent with previous estimates for Jupiter analogs (Cahoy et al. 2010). We further assume an edge-on inclination (90°) from the astrometric result provided in Section 6.2, and a HabEx Starshade mission concept configuration in the visible band (450-975 nm) (Gaudi et al. 2020). To account for the uncertainty in the inclination derivation from astrometry, we calculated flux ratio variation of the outer planet for inclinations from perfectly edge-on to face-on cases. The planet could achieve flux ratios larger than 10^{-10} , the required contrast ratio for HabEx (Gaudi et al. 2020), outside the inner working angle (IWA) for all inclination cases. But due to the high eccentricity nature of the orbit and the location of the periastron angle, the planet could have a maximum brightness with flux ratio around 9.5×10^{-9} near the edge of IWA for the 90° orbit. Figure 8 shows the top down view of the outer planet’s orbit. Flux ratio variation of the planet throughout its entire orbit for the edge-on case is color coded if the flux ratio is above 10^{-10} . Although the host star is a bit far (~ 41 pc) and dim (V mag ~ 8), the planet could potentially be imaged by future direct imaging missions when it approaches periastron, which will happen in about 10 years, thanks to its high planet-to-star flux ratio.

We also use the stellar properties from Stassun et al. (2019), shown in Table 2, to calculate the extent of the conservative and optimistic Habitable Zone (HZ) regions (Kasting Whitmire; Kane & Gelino 2012; Kopparapu et al. 2013, 2014; Kane et al. 2016). The conservative and optimistic HZ lie in the range 0.86–1.54 AU and 0.68–1.62 AU, respectively, and are represented in Figure 8 by the light and dark regions. The periastron passage of the outer planet passes close to the HZ, but does not enter the HZ region. As demonstrated by the dynamical results shown in Figure 2 and discussed in Section 5.2, this orbital architecture allows for the possibility of potential terrestrial planets within the HZ that are able to retain long-term stability. However, it is worth noting that such terrestrial planets may experience significant non-zero eccentricity variations due to the perturbations from the known outer planet, similar to the scenario of the HR 5183 system, described by Kane & Blunt (2019).

In that light, it is interesting to further examine the results of the detailed dynamical simulations described in Section 5, to examine the degree to which the ‘stable’ particles (which survived for the full duration of the simulations) were stirred or excited by the influence of the two known planets. In Figure 9, we therefore examine the degree to which

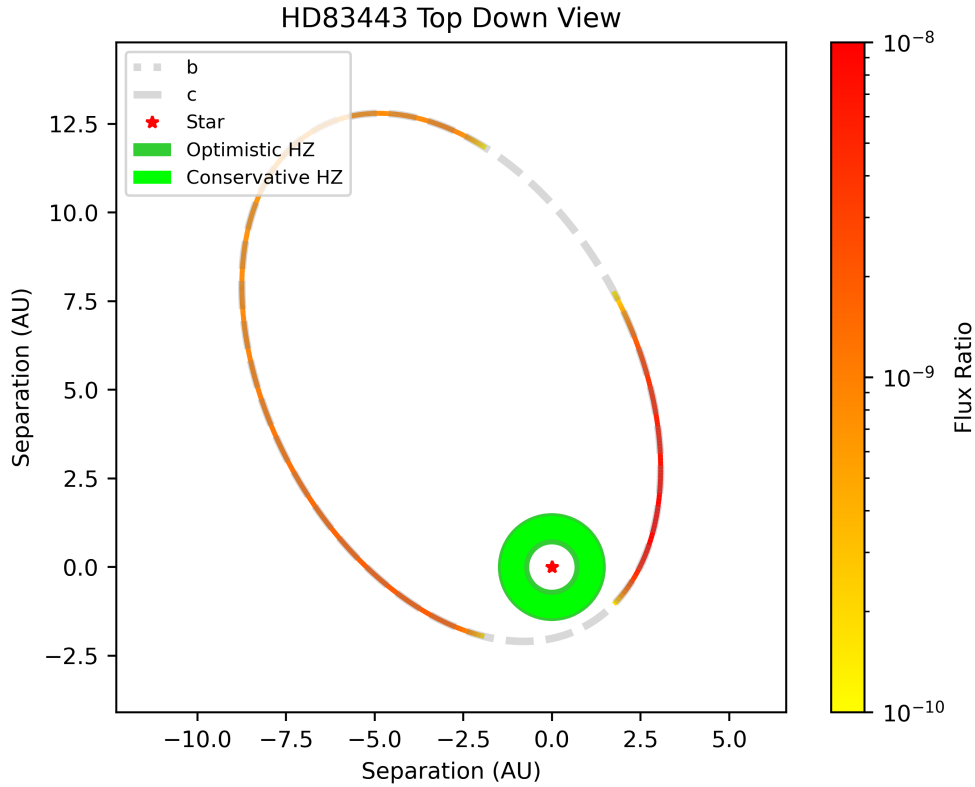


Figure 8. Top down view of the HD 83443 system with both conservative and optimistic HZ regions shown in light green and dark green, respectively. The orbit of the outer planet is color coded with the planet-to-star flux ratio if the brightness is above 1×10^{-10} , assuming near edge-on inclination. Part of the orbit with low flux ratios not color coded is due to the planet passing through the inner working angle of *HabEx* starshade. The inner b planet is not shown due to its proximity to the host star and the scale of the plot.

the orbits of the surviving test particles are stirred by the end of our simulations. In the panels of that figure, we show the difference between the initial and final semi-major axes (top, Δa) and eccentricities (bottom, Δe) for all particles that survive to the end of the simulations. It is immediately clear that all test particles that are on even moderately eccentric orbits in the inner reaches of the system only survive if they are either (a) trapped in mean-motion resonance with HD 83443 b, or (b) move on orbits exterior to the red dotted line - orbits whose closest approach to the orbit of the inner planet occurs at a distance of more than 5 Hill radii exterior to that planet’s orbit.

Both the Δa and Δe plots show a marked excitation just beneath the red dotted line - showing that particles are being ejected from the inner part of the system on orbits with constant pericentre located just beyond that location. This is not a surprise - encounters with HD 83443 b act to excite the orbital eccentricity of test particles, which in turn modifies their orbital semi-major axis, since the encounters are happening at, or near, the pericentre of the particle’s orbit. The result is that particles will random walk along that ejection line, with encounters increasing or decreasing the eccentricity and semi-major axis of the particle’s orbit until either it encounters HD 83443 c, and is shifted off that line, decoupling it from the influence of HD 83443 b, or until it is ejected from the system entirely as a result of a kick from HD 83443 b.

Such behaviour actually explains the population of test particles in the HZ of the HD 83443 system that display marked excitation in both a and e . Particles on highly eccentric orbits with $a \gtrsim 0.6$ au can experience relatively close encounters with both HD 83443 b (at pericentre) and HD 83443 c (at apoapse). The result is that particles ejected to that regime by HD 83443 b can be moved onto more circular orbits, within the HZ, by encounters with HD 83443 c - along the lines of constant apocentre distance denoted by the blue lines. As such, particles from the inner areas of the system can be temporarily trapped in the HZ. The reverse behaviour is also clearly true - particles originating

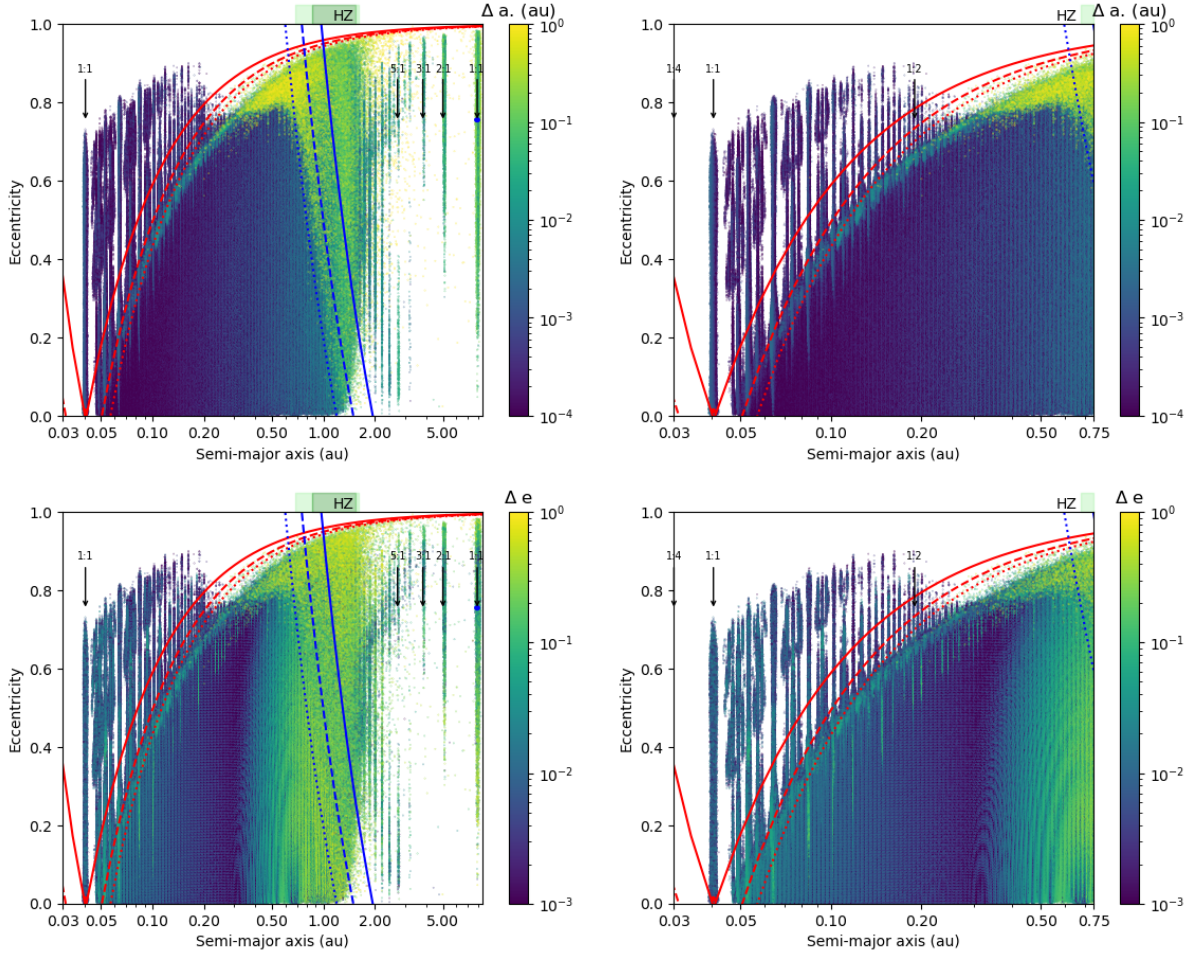


Figure 9. The amount of stirring experienced by the stable test particles that survived the full duration of our simulations of the HD 83443 system. Each individual dot plotted represents a test particle that survived until the end of our simulations. The top panels show, for each test particle, the difference between that particles initial and final semi-major axes (i.e. $\Delta a = |a_{init} - a_{final}|$), whilst the lower panels show the change, for each test particle, in orbital eccentricity (i.e. $\Delta e = |e_{init} - e_{final}|$). The left panels show the full range of semi-major axes considered in this work, whilst the right panel zooms in on the inner 0.75 au of the system, to show in more detail the fine structure in that region. The solid blue line connects all $a - e$ locations with apocentre at the pericentre of the orbit of HD 83443c, with the dashed and dotted blue lines marking orbits with apocentres one and three Hill radii interior to HD 83443c’s pericentre. Similarly, the solid red line connects all orbits with apocentre or pericentre at the orbit of HD 83443b, such that all objects within the wedge described by the solid red line move on orbits that cross that of that planet. The red dashed and red dotted lines show orbits with pericentre three and five Hill radii beyond the orbit of HD 83443b, respectively. Whilst orbits in the potential Habitable Zone around HD 83443 are stable (in that test particles in that region can survive the duration of the simulations), it is apparent that those particles experience significant stirring, primarily from HD 83443c, which would, at the very least, result in an planets in that region experiencing dramatic Milankovitch cycles, and may indicate that such orbits would prove unstable on longer timescales.

on orbits within 5 Hill radii of HD 83443c can be excited, by that planet, until their pericentre falls within 5 Hill radii of HD 83443b - which can then either help to eject those particles (moving them outward along the line of constant pericentre), or can drag them to smaller eccentricities along that line, decoupling them from the influence of HD 83443c.

The result is that the outer reaches of the HZ in the HD 83443 system is a chaotic place, dynamically stirred by HD 83443c to such a degree that it seems highly unlikely any planet mass objects could survive there on sufficiently stable orbits to be considered truly habitable. At low eccentricities, however, it is clear from Figure 9 that, at least in the inner part of the HZ, particles can survive on long timescales with only negligible stirring, and so, with the

system’s current architecture, one cannot rule out the presence of planets moving on stable orbits in the HZ of the system. Even in the inner reaches of the HZ, though, there is evidence of marked stirring in orbital eccentricity (with Δe values of ~ 0.1 or greater), which might suggest that, although planets in this region would be dynamically stable, they might nevertheless experience Milankovitch cycles of such amplitude as to render them effectively inhospitable. Should such planets eventually be discovered, simulations such as those described in Horner et al. (2020b) and Vervoort et al. (2022) will be vital to assess the severity of the climate variations that such behaviour would cause, and to help assess the degree to which those planets would be suitable target for follow-up observations.

6.4. *Origins of the HD 83443 system*

The origin of hot Jupiters is still a topic of much discussion. As described in the Introduction, there are three main mechanisms that are invoked to explain the presence of hot Jupiters, namely:

- The inward migration of a giant planet through interaction with circumstellar disk; typically maintaining low eccentricity and inclination throughout.
- One or more close encounters between two giant planets scattering those planets onto highly eccentric orbits, followed by tidal circularisation of the proto-hot Jupiter; typically results in low to moderate orbital inclinations for the hot Jupiter, and the presence of an outer planet on an eccentric orbit.
- Kozai-Lidov perturbations on the orbit of the proto-hot Jupiter from a distant, inclined stellar companion, followed by tidal circularisation; typically results in strongly misaligned hot Jupiters.

In this context, the presence of HD 83443 c in its highly eccentric orbit is of particular interest, since it points to the possibility that HD 83443 b achieved its current hot Jupiter status as a result of chaotic encounters with that outer planet (i.e., the second mechanism noted above). As a consequence, the remaining planet is left in a short and highly eccentric orbit (e.g. Rasio & Ford 1996; Weidenschilling & Marzari 1996; Chatterjee et al. 2008) and undergoes tidal circularisation (Nagasawa et al. 2008; Bonomo et al. 2017; Dong et al. 2021). Wu & Lithwick (2011) proposed a secular migration mechanism to explain the pile-up of hot Jupiters on ~ 3 -day orbits, the generally lower masses ($< 1 M_J$) of hot Jupiters, and the low frequency of additional planets in hot Jupiter systems within a few au (and noting that more distant eccentric companions were likely). The HD 83443 system, with a 3-day hot Jupiter and an eccentric outer planet, could be considered a textbook example of the type of system produced by secular migration. It is worth noting that the analysis given in Wu & Lithwick (2011) as well as Chatterjee et al. (2008) focused on systems initially containing three giant planets (where the third planet is ejected). The lack of further giant planets in the HD 83443 system is consistent with such a history. Figure 10 shows the distribution of “acquaintances of hot Jupiters”: systems containing a hot Jupiter and a distant exterior giant planet. Of particular relevance are those where the outer planet retains a high eccentricity. HD 83443c is now the most distant, highest-eccentricity such planet. Only WASP-53c is more eccentric at $e = 0.837$, although that object is a brown dwarf of at least $16.4 M_J$ (Triaud et al. 2017).

Many simulations and analysis have been done to reproduce the eccentricity distribution observed in the population of exoplanets, which includes the configuration of HD 83443 (e.g. Ford & Rasio 2008; Chatterjee et al. 2008; Raymond et al. 2010; Sotiriadis et al. 2017; Carrera et al. 2019; Bowler et al. 2020). The Kozai-Lidov mechanism (Kozai 1962; Lidov 1962) is often invoked to explain high-eccentricity planets (e.g. Desidera & Barbieri 2007; Wittenmyer et al. 2007b; Blunt et al. 2019; Venner et al. 2021). However, Kozai-Lidov oscillations, whereby orbital inclination is exchanged with eccentricity to produce high-eccentricity planets, require the influence of a binary stellar companion (Mustill et al. 2017). As shown in Section 6.2, there is no evidence for a stellar-mass object bound to HD 83443. We must instead look to an ancient and dramatic dynamical event to assign responsibility for the configuration of the HD 83443 system.

For systems in which many giant planets initially form, those planets perturb each other, which can result in eccentricity excitation and the possible ejection of planets by close dynamical encounters (e.g. Rasio & Ford 1996; Weidenschilling & Marzari 1996; Lin & Ida 1997; Ford & Rasio 2008). Carrera et al. (2019) showed that planet-planet scattering can result in final eccentricities even as high as 0.999. A scattering origin for the current orbits of the two planets in the HD 83443 system would suggest that, despite the broad areas of stability revealed in the dynamical analysis described in Section 5, the presence of additional planets between the two described in this work is unlikely. Such planets would likely have been ejected or devoured through collisions during the period that the orbit of HD 83443 b was highly eccentric, particularly given that its orbital semi-major axis (and thus the location of all its associated mean-motion resonances) would have swept through the ‘stable’ region revealed by those simulations.

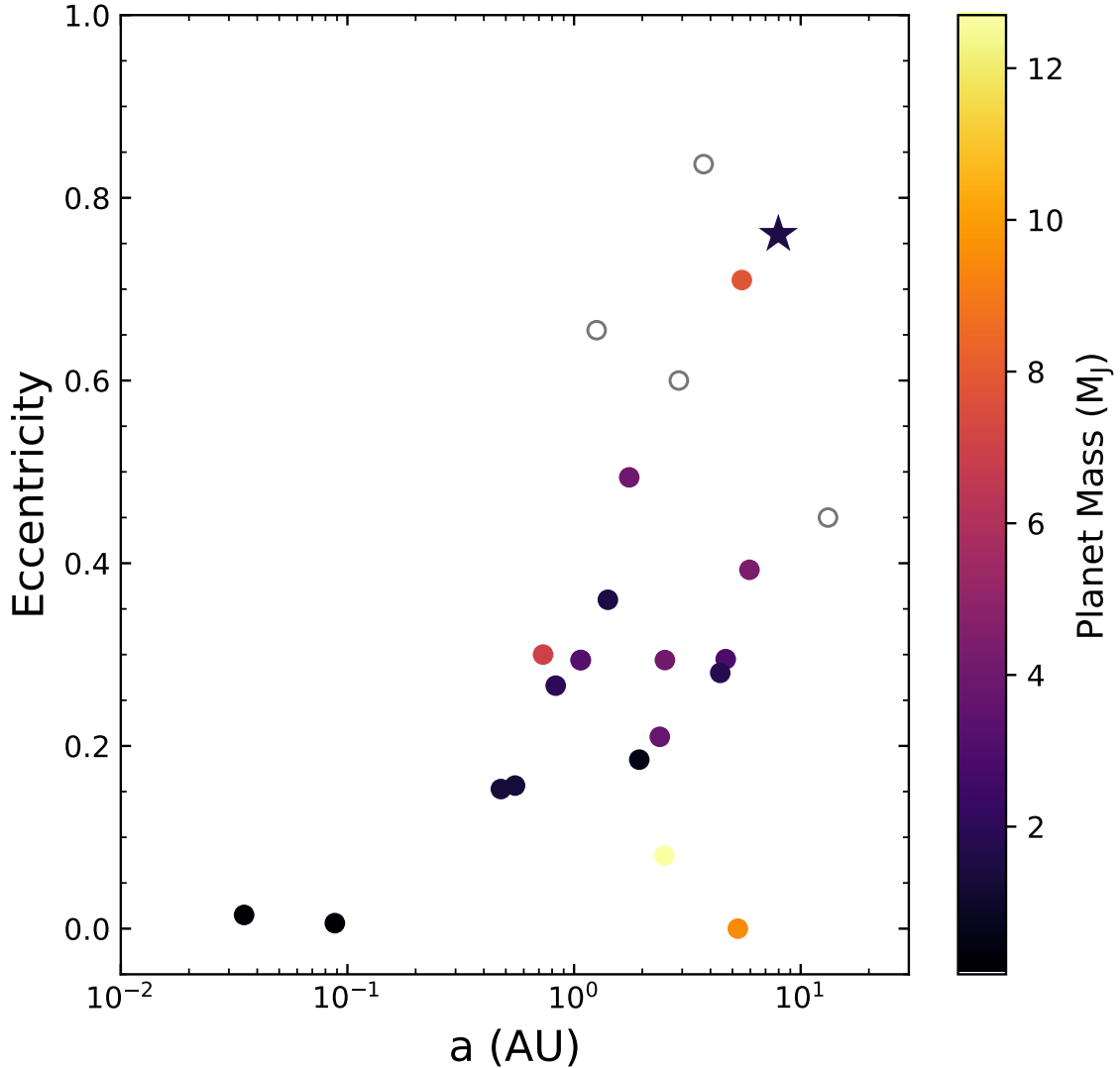


Figure 10. Eccentricity-semimajor axis distribution of exterior companions to Hot Jupiters. HD 83443c is shown as a star, and is the most distant, most eccentric such planet yet found. Each planet is color-coded by its planetary mass value (or projected mass value if no radius measurement). The open circles represent known brown dwarf exterior companions. Planet data from NASA Exoplanet Archive, accessed 2021 Nov 15.

Dawson & Murray-Clay (2013) showed that metal-rich stars hosted more hot Jupiters and more highly eccentric giant planets; the HD 83443 system satisfies all of these characteristics. By comparison, the 14 Herculis system, with two giant planets (Wittenmyer et al. 2007a; Rosenthal et al. 2021), was recently fully characterised by Bardalez Gagliuffi et al. (2021) with a combination of long-term radial velocity and astrometry. The outer planet was found to have a high eccentricity ($e = 0.64_{-0.13}^{+0.12}$) and to be significantly misaligned with the inner planet. Much like for HD 83443, the evidence strongly supports a scattering origin for the configuration of the 14 Her system. In the absence of Kozai-Lidov oscillations to drive eccentricity, it is highly probable that HD 83443c arrived at its present location by a scattering event. It is interesting to note that scattering events would logically send the less-massive planet outward (as seems to be the case for 14 Her), yet for HD 83443 the outer planet is by a factor of ~ 3 the more massive of the two. This suggests that perhaps a third, even less massive ($< 0.4 M_J$) planet may have participated in the scattering and was ejected.

7. CONCLUSIONS

We have combined more than 20 years of precise radial-velocity data from four instruments to detect a highly eccentric giant planet in a 22.6-year orbit around the nearby K dwarf HD 83443. The orbit of HD 83443c is consistent with the 4σ positive linear trend noted by Wright et al. (2007). We use the non-detection of astrometric acceleration to place a firm upper limit on the true mass of HD 83443c, and with a joint fit of the radial velocities and astrometry we obtain a dynamical mass of $1.5_{-0.2}^{+0.5} M_J$. This system was already known to host a Hot Jupiter, and is a rare example of a planetary system with a Hot Jupiter and a second giant planet. The observed rarity of such objects is likely driven by the strong observational bias against the radial velocity detection of planets beyond ~ 8 -10 au; imaging studies have derived occurrence rates of $\sim 50\%$ for such companions (Knutson et al. 2014; Bryan et al. 2016). HD 83443c is reminiscent of the HR 5183 system (Kane & Blunt 2019), in which a high-eccentricity giant planet exerts its dynamical influence to sweep clean a vast region. The inner ~ 1 au, including the HZ of this K0V star, remains stable to the presence of additional undetected planets. We have shown that the inner Hot Jupiter does not transit in *TESS* photometry. The available astrometric data do not indicate any stellar-mass companions, further supporting the planetary interpretation of the radial velocity signal and suggesting emplacement in its current high-eccentricity orbit by planet-planet scattering rather than by the Kozai-Lidov mechanism. While HD 83443c is beyond the grasp of planned imaging missions, it remains a fascinating example of a well-characterised system containing both a hot Jupiter and a highly eccentric giant planet.

ACKNOWLEDGMENTS

MINERVA-Australis is supported by Australian Research Council LIEF Grant LE160100001, Discovery Grants DP180100972 and DP220100365, Mount Cuba Astronomical Foundation, and institutional partners University of Southern Queensland, UNSW Sydney, MIT, Nanjing University, George Mason University, University of Louisville, University of California Riverside, University of Florida, and The University of Texas at Austin.

We respectfully acknowledge the traditional custodians of all lands throughout Australia, and recognise their continued cultural and spiritual connection to the land, waterways, cosmos, and community. We pay our deepest respects to all Elders, ancestors and descendants of the Giabal, Jarowair, and Kambuwal nations, upon whose lands the MINERVA-Australis facility at Mt Kent is situated.

B.A. is supported by Australian Research Council Discovery Grant DP180100972. G. M. B. is supported by the National Science Foundation (NSF) Graduate Research Fellowship under grant no. 1650114.

T.F. acknowledges support from the University of California President’s Postdoctoral Fellowship Program.

This paper includes data collected with the *TESS* mission, obtained from the MAST data archive at the Space Telescope Science Institute (STScI). Funding for the *TESS* mission is provided by the NASA Explorer Program. STScI is operated by the Association of Universities for Research in Astronomy, Inc., under NASA contract NAS 5-26555.

This publication makes use of The Data & Analysis Center for Exoplanets (DACE), which is a facility based at the University of Geneva (CH) dedicated to extrasolar planets data visualisation, exchange and analysis. DACE is a platform of the Swiss National Centre of Competence in Research (NCCR) PlanetS, federating the Swiss expertise in Exoplanet research. The DACE platform is available at <https://dace.unige.ch>.

Facilities: TESS, MINERVA-Australis, AAT

Software: AstroImageJ (Collins et al. 2017), Exo-striker, (Trifonov 2019), emcee (Foreman-Mackey et al. 2013), htof (Brandt et al. 2021b,c), orvara (Brandt et al. 2021d), ptmcee (Foreman-Mackey et al. 2013; Vousden et al. 2016)

REFERENCES

- Addison, B., Wright, D. J., Wittenmyer, R. A., et al. 2019, *PASP*, 131, 115003. doi:10.1088/1538-3873/ab03aa
- Addison, B. C., Wright, D. J., Nicholson, B. A., et al. 2021, *MNRAS*, 502, 3704. doi:10.1093/mnras/staa3960
- Alibert, Y., Mordasini, C., Benz, W., et al. 2005a, *A&A*, 434, 343. doi:10.1051/0004-6361:20042032
- Alibert, Y., Mousis, O., Mordasini, C., et al. 2005b, *ApJL*, 626, L57. doi:10.1086/431325
- Alibert, Y., Broeg, C., Benz, W., et al. 2010, *Astrobiology*, 10, 19. doi:10.1089/ast.2009.0372
- Artymowicz, P. 2004, *Debris Disks and the Formation of Planets*, 324, 39
- Baraffe, I., Selsis, F., Chabrier, G., et al. 2004, *A&A*, 419, L13. doi:10.1051/0004-6361:20040129
- Bardalez Gagliuffi, D. C., Faherty, J. K., Li, Y., et al. 2021, arXiv:2111.06004
- Barnes, S. I., Gibson, S., Nield, K., et al. 2012, *Proc. SPIE*, 8446, 844688. doi:10.1117/12.926527
- Baruteau, C., Crida, A., Paardekooper, S.-J., et al. 2014, *Protostars and Planets VI*, 667. doi:10.2458/azu_uapress_9780816531240-ch029
- Batygin, K., Bodenheimer, P. H., & Laughlin, G. P. 2016, *ApJ*, 829, 114. doi:10.3847/0004-637X/829/2/114
- Bitsch, B., Crida, A., Libert, A.-S., et al. 2013, *A&A*, 555, A124. doi:10.1051/0004-6361/201220310
- Blunt, S., Endl, M., Weiss, L. M., et al. 2019, *AJ*, 158, 181. doi:10.3847/1538-3881/ab3e63
- Bodenheimer, P. 1997, *From Stardust to Planetesimals*, 122, 37
- Bodenheimer, P., Hubickyj, O., & Lissauer, J. J. 2000, *Icarus*, 143, 2. doi:10.1006/icar.1999.6246
- Boley, A. C., Granados Contreras, A. P., & Gladman, B. 2016, *ApJL*, 817, L17. doi:10.3847/2041-8205/817/2/L17
- Bonomo, A. S., Desidera, S., Benatti, S., et al. 2017, *A&A*, 602, A107. doi:10.1051/0004-6361/201629882
- Boss, A. P. 1997, *Science*, 276, 1836. doi:10.1126/science.276.5320.1836
- Boss, A. P. 1998, *Earth Moon and Planets*, 81, 19
- Boss, A. P. 2003, *ApJ*, 599, 577. doi:10.1086/379163
- Boss, A. P. 2006, *ISSI Scientific Reports Series*, 6, 287
- Bowler, B. P., Blunt, S. C., & Nielsen, E. L. 2020, *AJ*, 159, 63. doi:10.3847/1538-3881/ab5b11
- Brandt, G. M., Brandt, T. D., Dupuy, T. J., et al. 2021, *ApJL*, 915, L16. doi:10.3847/2041-8213/ac0540
- Brandt, G. M., Michalik, D., Brandt, T. D., et al. 2021, arXiv:2109.06761
- Brandt, G. M., Michalik, D., Andreason, T. 2021, 1.0.1, *Zenodo*, doi: 10.5281/zenodo.5534833
- Brandt, T. D., Dupuy, T. J., Li, Y., et al. 2021, *AJ*, 162, 186. doi:10.3847/1538-3881/ac042e
- Brandt, G. M., Dupuy, T. J., Li, Y., et al. 2021, arXiv:2109.07525
- Brandt, T. D. 2021, *ApJS*, 254, 42. doi:10.3847/1538-4365/abf93c
- Brandt, T. D. 2018, *ApJS*, 239, 31. doi:10.3847/1538-4365/aaec06
- Bryan, M. L., Knutson, H. A., Howard, A. W., et al. 2016, *ApJ*, 821, 89. doi:10.3847/0004-637X/821/2/89
- Butler, R. P., Marcy, G. W., Vogt, S. S., et al. 2002, *ApJ*, 578, 565. doi:10.1086/342471
- Butler, R. P., Vogt, S. S., Laughlin, G., et al. 2017, *AJ*, 153, 208. doi:10.3847/1538-3881/aa66ca
- Cahoy, K. L., Marley, M. S., & Fortney, J. J. 2010, *ApJ*, 724, 189. doi:10.1088/0004-637X/724/1/189
- Cameron, A. G. W. 1978, *Moon and Planets*, 18, 5. doi:10.1007/BF00896696
- Carrera, D., Raymond, S. N., & Davies, M. B. 2019, *A&A*, 629, L7. doi:10.1051/0004-6361/201935744
- Chambers, J. E. 1999, *MNRAS*, 304, 793. doi:10.1046/j.1365-8711.1999.02379.x
- Chambers, J. E. 2004, *Earth and Planetary Science Letters*, 223, 241. doi:10.1016/j.epsl.2004.04.031
- Chatterjee, S., Ford, E. B., Matsumura, S., et al. 2008, *ApJ*, 686, 580. doi:10.1086/590227
- Chen, J. & Kipping, D. 2017, *ApJ*, 834, 17. doi:10.3847/1538-4357/834/1/17
- Collins, K. A., Kielkopf, J. F., Stassun, K. G., et al. 2017, *AJ*, 153, 77. doi:10.3847/1538-3881/153/2/77
- Dalal, S., Hébrard, G., Lecavelier des Étangs, A., et al. 2019, *A&A*, 631, A28. doi:10.1051/0004-6361/201935944
- Dawson, R. I. & Johnson, J. A. 2018, *ARA&A*, 56, 175. doi:10.1146/annurev-astro-081817-051853
- Dawson, R. I. & Murray-Clay, R. A. 2013, *ApJL*, 767, L24. doi:10.1088/2041-8205/767/2/L24
- Delgado Mena, E., Moya, A., Adibekyan, V., et al. 2019, *A&A*, 624, A78. doi:10.1051/0004-6361/201834783
- Desidera, S. & Barbieri, M. 2007, *A&A*, 462, 345. doi:10.1051/0004-6361:20066319
- Dong, J., Huang, C. X., Zhou, G., et al. 2021, *ApJL*, 920, L16. doi:10.3847/2041-8213/ac2600
- Dupuy, T. J., Brandt, G. M., & Brandt, T. D. 2021, arXiv:2110.13173
- Endl, M., Bergmann, C., Hearnshaw, J., et al. 2015, *International Journal of Astrobiology*, 14, 305. doi:10.1017/S1473550414000081

- Érdi, B. & Sándor, Z. 2005, *Celestial Mechanics and Dynamical Astronomy*, 92, 113.
doi:10.1007/s10569-004-3114-5
- Fabrycky, D. C. & Winn, J. N. 2009, *ApJ*, 696, 1230.
doi:10.1088/0004-637X/696/2/1230
- Fischer, D. A. & Valenti, J. 2005, *ApJ*, 622, 1102.
doi:10.1086/428383
- Ford, E. B. & Rasio, F. A. 2008, *ApJ*, 686, 621.
doi:10.1086/590926
- Foreman-Mackey, D., Hogg, D. W., Lang, D., et al. 2013, *PASP*, 125, 306. doi:10.1086/670067
- Fulton, B. J., Rosenthal, L. J., Hirsch, L. A., et al. 2021, *ApJS*, 255, 14. doi:10.3847/1538-4365/abfcc1
- Gaia Collaboration 2018, *VizieR Online Data Catalog*, I/345
- Gaia Collaboration, Brown, A. G. A., Vallenari, A., et al. 2018, *A&A*, 616, A1. doi:10.1051/0004-6361/201833051
- Gaudi, B. S., Seager, S., Mennesson, B., et al. 2020, *arXiv:2001.06683*
- Ghezzi, L., Cunha, K., Smith, V. V., et al. 2010, *ApJ*, 720, 1290. doi:10.1088/0004-637X/720/2/1290
- Ghezzi, L., Montet, B. T., & Johnson, J. A. 2018, *ApJ*, 860, 109. doi:10.3847/1538-4357/aac37c
- Gilmore, J. B. & Ross, A. 2008, *PhRvD*, 78, 124021.
doi:10.1103/PhysRevD.78.124021
- Goldreich, P. & Tremaine, S. 1980, *ApJ*, 241, 425.
doi:10.1086/158356
- Gomes, R. S. 1997, *AJ*, 114, 396. doi:10.1086/118483
- Hasegawa, Y., Yu, T. Y. M., & Hansen, B. M. S. 2019, *A&A*, 629, L1. doi:10.1051/0004-6361/201936138
- Heller, R. 2019, *A&A*, 628, A42.
doi:10.1051/0004-6361/201833486
- Holt, T. R., Horner, J., Nesvorný, D., et al. 2021, *MNRAS*, 504, 1571. doi:10.1093/mnras/stab894
- Horner, J. & Lykawka, P. S. 2010, *MNRAS*, 405, 49.
doi:10.1111/j.1365-2966.2010.16441.x
- Horner, J., Marshall, J. P., Wittenmyer, R. A., et al. 2011, *MNRAS*, 416, L11. doi:10.1111/j.1745-3933.2011.01087.x
- Horner, J., Wittenmyer, R. A., Hinse, T. C., et al. 2013, *MNRAS*, 435, 2033. doi:10.1093/mnras/stt1420
- Horner, J., Kane, S. R., Marshall, J. P., et al. 2020, *PASP*, 132, 102001. doi:10.1088/1538-3873/ab8eb9
- Horner, J., Vervoort, P., Kane, S. R., et al. 2020, *AJ*, 159, 10. doi:10.3847/1538-3881/ab5365
- Horner, J., Marshall, J. P., Wittenmyer, R. A., et al. 2022, *AJ*, submitted
- Houk, N. 1978, *Ann Arbor : Dept. of Astronomy, University of Michigan : distributed by University Microfilms International*, 1978-
- Jenkins, J. M., Twicken, J. D., McCauliff, S., et al. 2016, *Proc. SPIE*, 9913, 99133E. doi:10.1117/12.2233418
- Jewitt, D. C., Trujillo, C. A., & Luu, J. X. 2000, *AJ*, 120, 1140. doi:10.1086/301453
- Johansen, A., Oishi, J. S., Mac Low, M.-M., et al. 2007, *Nature*, 448, 1022. doi:10.1038/nature06086
- Jones, M. I., Jenkins, J. S., Brahm, R., et al. 2016, *A&A*, 590, A38. doi:10.1051/0004-6361/201628067
- Kane, S. R. & Gelino, D. M. 2012, *Astrobiology*, 12, 940.
doi:10.1089/ast.2011.0798
- Kane, S. R. 2013, *ApJ*, 766, 10.
doi:10.1088/0004-637X/766/1/10
- Kane, S. R., Hill, M. L., Kasting, J. F., et al. 2016, *ApJ*, 830, 1. doi:10.3847/0004-637X/830/1/1
- Kane, S. R., Meshkat, T., & Turnbull, M. C. 2018, *AJ*, 156, 267. doi:10.3847/1538-3881/aae981
- Kane, S. R. & Blunt, S. 2019, *AJ*, 158, 209.
doi:10.3847/1538-3881/ab4c3e
- Kane, S. R., Fetherolf, T., & Hill, M. L. 2020, *AJ*, 159, 176.
doi:10.3847/1538-3881/ab7818
- Kasting J. F., Whitmire D. P., Reynolds R. T., 1993, *Icar*, 101, 108. doi:10.1006/icar.1993.1010
- Knutson, H. A., Fulton, B. J., Montet, B. T., et al. 2014, *ApJ*, 785, 126. doi:10.1088/0004-637X/785/2/126
- Kopparapu, R. K., Ramirez, R., Kasting, J. F., et al. 2013, *ApJ*, 765, 131. doi:10.1088/0004-637X/765/2/131
- Kopparapu, R. K., Ramirez, R. M., SchottelKotte, J., et al. 2014, *ApJL*, 787, L29. doi:10.1088/2041-8205/787/2/L29
- Kozai, Y. 1962, *AJ*, 67, 591. doi:10.1086/108790
- Lam, K. W. F., Korth, J., Masuda, K., et al. 2020, *AJ*, 159, 120. doi:10.3847/1538-3881/ab66c9
- Leleu, A., Lillo-Box, J., Sestovic, M., et al. 2019, *A&A*, 624, A46. doi:10.1051/0004-6361/201834901
- Leleu, A., Alibert, Y., Hara, N. C., et al. 2021, *A&A*, 649, A26. doi:10.1051/0004-6361/202039767
- Levison, H. F., Shoemaker, E. M., & Shoemaker, C. S. 1997, *Nature*, 385, 42. doi:10.1038/385042a0
- Li, Y., Brandt, T. D., Brandt, G. M., et al. 2021, *arXiv:2109.10422*
- Li, Z., Hildebrandt, S. R., Kane, S. R., et al. 2021, *AJ*, 162, 9. doi:10.3847/1538-3881/abf831
- Lin, D. N. C. & Papaloizou, J. 1986, *ApJ*, 309, 846.
doi:10.1086/164653
- Lidov, M. L. 1962, *Planet. Space Sci.*, 9, 719.
doi:10.1016/0032-0633(62)90129-0
- Lin, D. N. C. & Ida, S. 1997, *ApJ*, 477, 781.
doi:10.1086/303738
- Lin, D. N. C., Bodenheimer, P., & Richardson, D. C. 1996, *Nature*, 380, 606. doi:10.1038/380606a0

- Lo Curto, G., Pepe, F., Avila, G., et al. 2015, *The Messenger*, 162, 9
- Luger, R., Sestovic, M., Kruse, E., et al. 2017, *Nature Astronomy*, 1, 0129. doi:10.1038/s41550-017-0129
- Lykawka, P. S. & Horner, J. 2010, *MNRAS*, 405, 1375. doi:10.1111/j.1365-2966.2010.16538.x
- Madhusudhan, N. & Winn, J. N. 2009, *ApJ*, 693, 784. doi:10.1088/0004-637X/693/1/784
- Malhotra, R. 1993, *Icarus*, 106, 264. doi:10.1006/icar.1993.1170
- Mannings, V., Boss, A. P., & Russell, S. S. 2000, *Protostars and Planets IV*
- Masset, F. S. & Papaloizou, J. C. B. 2003, *ApJ*, 588, 494. doi:10.1086/373892
- Mayor, M., Pepe, F., Queloz, D., et al. 2003, *The Messenger*, 114, 20
- Mayor, M., Udry, S., Naef, D., et al. 2004, *A&A*, 415, 391. doi:10.1051/0004-6361:20034250
- Mayor, M., Naef, D., Pepe, F., et al. 2004, *Planetary Systems in the Universe*, 202, 84
- Minton, D. A. & Malhotra, R. 2009, *Nature*, 457, 1109. doi:10.1038/nature07778
- Minton, D. A. & Malhotra, R. 2011, *ApJ*, 732, 53. doi:10.1088/0004-637X/732/1/53
- Morbidelli, A., Levison, H. F., Tsiganis, K., et al. 2005, *Nature*, 435, 462. doi:10.1038/nature03540
- Mordasini, C., Alibert, Y., & Benz, W. 2009a, *A&A*, 501, 1139. doi:10.1051/0004-6361/200810301
- Mordasini, C., Alibert, Y., Benz, W., et al. 2009b, *A&A*, 501, 1161. doi:10.1051/0004-6361/200810697
- Murray, N., Hansen, B., Holman, M., et al. 1998, *Science*, 279, 69. doi:10.1126/science.279.5347.69.
- Mustill, A. J., Davies, M. B., & Johansen, A. 2017, *MNRAS*, 468, 3000. doi:10.1093/mnras/stx693
- Nagasawa, M., Ida, S., & Bessho, T. 2008, *ApJ*, 678, 498. doi:10.1086/529369
- Naoz, S., Farr, W. M., Lithwick, Y., et al. 2011, *Nature*, 473, 187. doi:10.1038/nature10076
- Nesvorný, D., Vokrouhlický, D., & Morbidelli, A. 2013, *ApJ*, 768, 45. doi:10.1088/0004-637X/768/1/45
- Osborn, A. & Bayliss, D. 2020, *MNRAS*, 491, 4481. doi:10.1093/mnras/stz3207
- Papaloizou, J. & Lin, D. N. C. 1984, *ApJ*, 285, 818. doi:10.1086/162561
- Papaloizou, J. C. B. & Terquem, C. 2006, *Reports on Progress in Physics*, 69, 119. doi:10.1088/0034-4885/69/1/R03
- Papaloizou, J. C. B. & Terquem, C. 1999, *ApJ*, 521, 823. doi:10.1086/307581
- Perri, F. & Cameron, A. G. W. 1974, *Icarus*, 22, 416. doi:10.1016/0019-1035(74)90074-8
- Perryman, M., Hartman, J., Bakos, G. Á., et al. 2014, *ApJ*, 797, 14. doi:10.1088/0004-637X/797/1/14
- Perryman, M. 2018, *The Exoplanet Handbook* by Michael Perryman, Cambridge University Press; Second Edition, 952 p., ISBN: 9781108419772
- Pirani, S., Johansen, A., Bitsch, B., et al. 2019, *A&A*, 623, A169. doi:10.1051/0004-6361/201833713
- Pollack, J. B., Hubickyj, O., Bodenheimer, P., et al. 1996, *Icarus*, 124, 62. doi:10.1006/icar.1996.0190
- Rasio, F. A. & Ford, E. B. 1996, *Science*, 274, 954. doi:10.1126/science.274.5289.954
- Raymond, S. N., Armitage, P. J., & Gorelick, N. 2010, *ApJ*, 711, 772. doi:10.1088/0004-637X/711/2/772
- Righter, K. & O'Brien, D. P. 2011, *Proceedings of the National Academy of Science*, 108, 19165. doi:10.1073/pnas.1013480108
- Romero-Wolf, A., Bryden, G., Seager, S., et al. 2021, *Journal of Astronomical Telescopes, Instruments, and Systems*, 7, 021210. doi:10.1117/1.JATIS.7.2.021210
- Rosenthal, L. J., Fulton, B. J., Hirsch, L. A., et al. 2021, *ApJS*, 255, 8. doi:10.3847/1538-4365/abe23c
- Rowan, D., Meschiari, S., Laughlin, G., et al. 2016, *ApJ*, 817, 104. doi:10.3847/0004-637X/817/2/104
- Santos, N. C., Israelian, G., & Mayor, M. 2004, *A&A*, 415, 1153. doi:10.1051/0004-6361:20034469
- Schwarz, R., Dvorak, R., Süli, Á., et al. 2007, *A&A*, 474, 1023. doi:10.1051/0004-6361:20077994
- Seager, S., Kasdin, N. J., Booth, J., et al. 2019, *BAAS*
- Shallue, C. J. & Vanderburg, A. 2018, *AJ*, 155, 94. doi:10.3847/1538-3881/aa9e09
- Sotiriadis, S., Libert, A.-S., Bitsch, B., et al. 2017, *A&A*, 598, A70. doi:10.1051/0004-6361/201628470
- Sousa, S. G., Santos, N. C., Mayor, M., et al. 2008, *A&A*, 487, 373. doi:10.1051/0004-6361:200809698
- Stassun, K. G., Collins, K. A., & Gaudi, B. S. 2017, *AJ*, 153, 136. doi:10.3847/1538-3881/aa5df3
- Stassun, K. G., Oelkers, R. J., Paegert, M., et al. 2019, *AJ*, 158, 138. doi:10.3847/1538-3881/ab3467
- Tal-Or, L., Trifonov, T., Zucker, S., et al. 2019, *MNRAS*, 484, L8. doi:10.1093/mnrasl/sly227
- Tanaka, H., Takeuchi, T., & Ward, W. R. 2002, *ApJ*, 565, 1257. doi:10.1086/324713
- Tinney, C. G., Butler, R. P., Marcy, G. W., et al. 2001, *ApJ*, 551, 507. doi:10.1086/320097
- Tinney, C. G., Wittenmyer, R. A., Butler, R. P., et al. 2011, *ApJ*, 732, 31. doi:10.1088/0004-637X/732/1/31
- TriAUD, A. H. M. J., Neveu-VanMalle, M., Lendl, M., et al. 2017, *MNRAS*, 467, 1714. doi:10.1093/mnras/stx154

- Trifonov, T. 2019, *Astrophysics Source Code Library*, ascl:1906.004
- Trifonov, T., Tal-Or, L., Zechmeister, M., et al. 2020, *A&A*, 636, A74. doi:10.1051/0004-6361/201936686
- Trilling, D. E., Lunine, J. I., & Benz, W. 2002, *A&A*, 394, 241. doi:10.1051/0004-6361:20021108
- Turnbull, M. C., Zimmerman, N., Girard, J. H., et al. 2021, *Journal of Astronomical Telescopes, Instruments, and Systems*, 7, 021218. doi:10.1117/1.JATIS.7.2.021218
- Valenti, J. A. & Fischer, D. A. 2005, *ApJS*, 159, 141. doi:10.1086/430500
- Vervoort, P., Horner, J., Kane, S. R., Kirtland Turner, S. & Gilmore, J. B. 2022, submitted to *AJ*
- Venner, A., Pearce, L. A., & Vanderburg, A. 2021, arXiv:2111.03676
- Vidal-Madjar, A., Lecavelier des Etangs, A., Désert, J.-M., et al. 2003, *Nature*, 422, 143. doi:10.1038/nature01448
- Vousden, W. D., Farr, W. M., & Mandel, I. 2016, *MNRAS*, 455, 1919. doi:10.1093/mnras/stv2422
- Ward, W. R. 1986, *Icarus*, 67, 164. doi:10.1016/0019-1035(86)90182-X
- Ward, W. R. 1997a, *Icarus*, 126, 261. doi:10.1006/icar.1996.5647
- Ward, W. R. 1997b, *ApJL*, 482, L211. doi:10.1086/310701
- Weidenschilling, S. J. & Marzari, F. 1996, *Nature*, 384, 619. doi:10.1038/384619a0
- Wetherill, G. W. 1990, *Annual Review of Earth and Planetary Sciences*, 18, 205. doi:10.1146/annurev.ea.18.050190.001225
- Winn, J. N., Johnson, J. A., Albrecht, S., et al. 2009, *ApJL*, 703, L99. doi:10.1088/0004-637X/703/2/L99
- Wittenmyer, R. A., Endl, M., Cochran, W. D., et al. 2006, *AJ*, 132, 177. doi:10.1086/504942
- Wittenmyer, R. A., Endl, M., & Cochran, W. D. 2007a, *ApJ*, 654, 625. doi:10.1086/509110
- Wittenmyer, R. A., Endl, M., Cochran, W. D., et al. 2007b, *AJ*, 134, 1276. doi:10.1086/520880
- Wittenmyer, R. A., Endl, M., Cochran, W. D., et al. 2009, *ApJS*, 182, 97. doi:10.1088/0067-0049/182/1/97
- Wittenmyer, R. A., Horner, J., Tinney, C. G., et al. 2014, *ApJ*, 783, 103. doi:10.1088/0004-637X/783/2/103
- Wittenmyer, R. A., Butler, R. P., Tinney, C. G., et al. 2016, *ApJ*, 819, 28. doi:10.3847/0004-637X/819/1/28
- Wittenmyer, R. A., Jones, M. I., Zhao, J., et al. 2017, *AJ*, 153, 51. doi:10.3847/1538-3881/153/2/51
- Wittenmyer, R. A., Horner, J., Mengel, M. W., et al. 2017, *AJ*, 153, 167. doi:10.3847/1538-3881/aa5f17
- Wittenmyer, R. A., Horner, J., Carter, B. D., et al. 2018, arXiv:1806.09282
- Wittenmyer, R. A., Wang, S., Horner, J., et al. 2020, *MNRAS*, 492, 377. doi:10.1093/mnras/stz3436
- Wong, I., Shporer, A., Daylan, T., et al. 2020, *AJ*, 160, 155. doi:10.3847/1538-3881/ababad
- Wong, I., Kitzmann, D., Shporer, A., et al. 2021, *AJ*, 162, 127. doi:10.3847/1538-3881/ac0c7d
- Wright, J. T., Marcy, G. W., Fischer, D. A., et al. 2007, *ApJ*, 657, 533. doi:10.1086/510553
- Wu, Y. & Lithwick, Y. 2011, *ApJ*, 735, 109. doi:10.1088/0004-637X/735/2/109
- Zechmeister, M., Kürster, M., Endl, M., et al. 2013, *A&A*, 552, A78. doi:10.1051/0004-6361/201116551

A. CORNERPLOTS

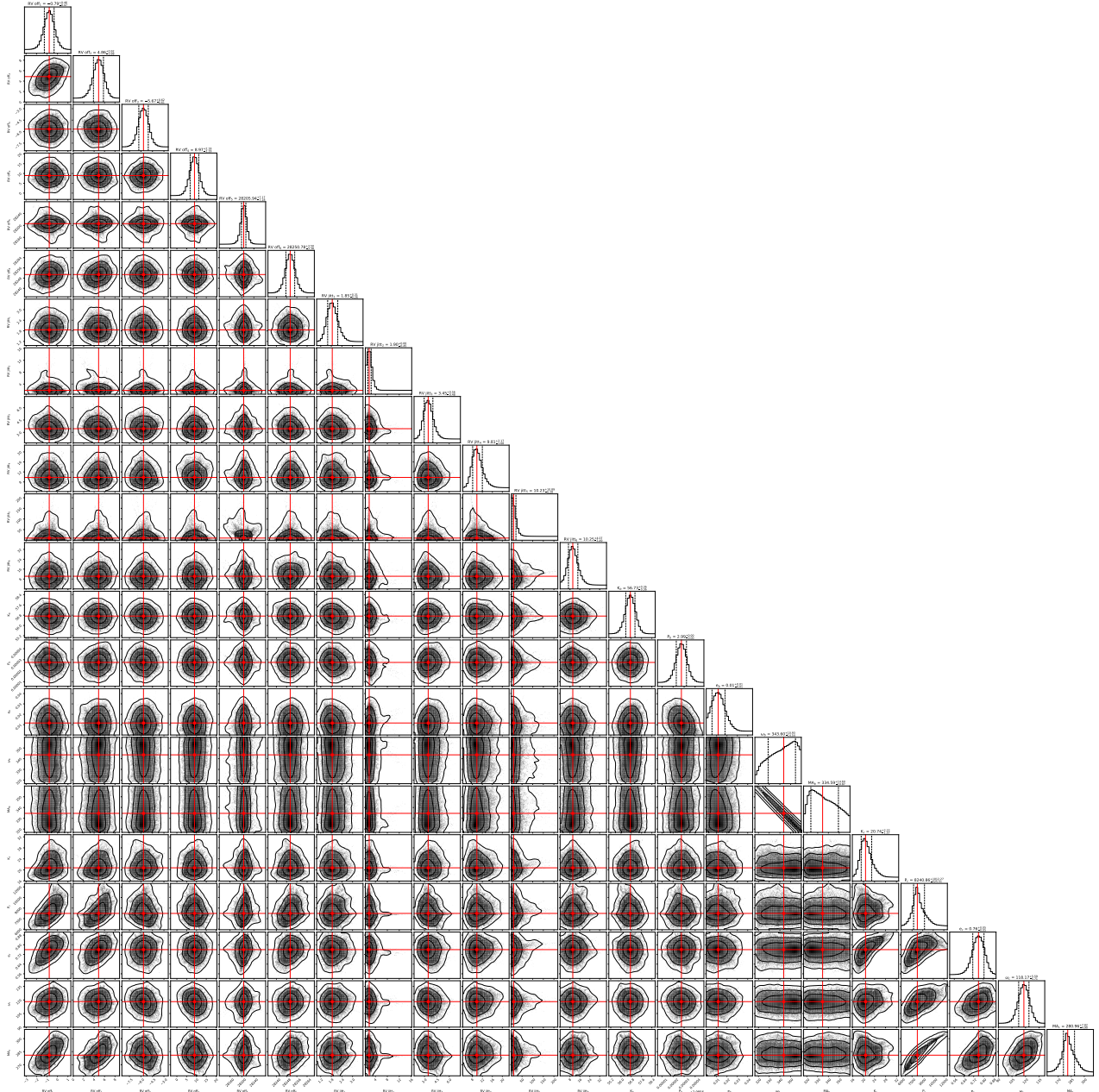


Figure 11. Corner plot - starting orbital period: 6000 days

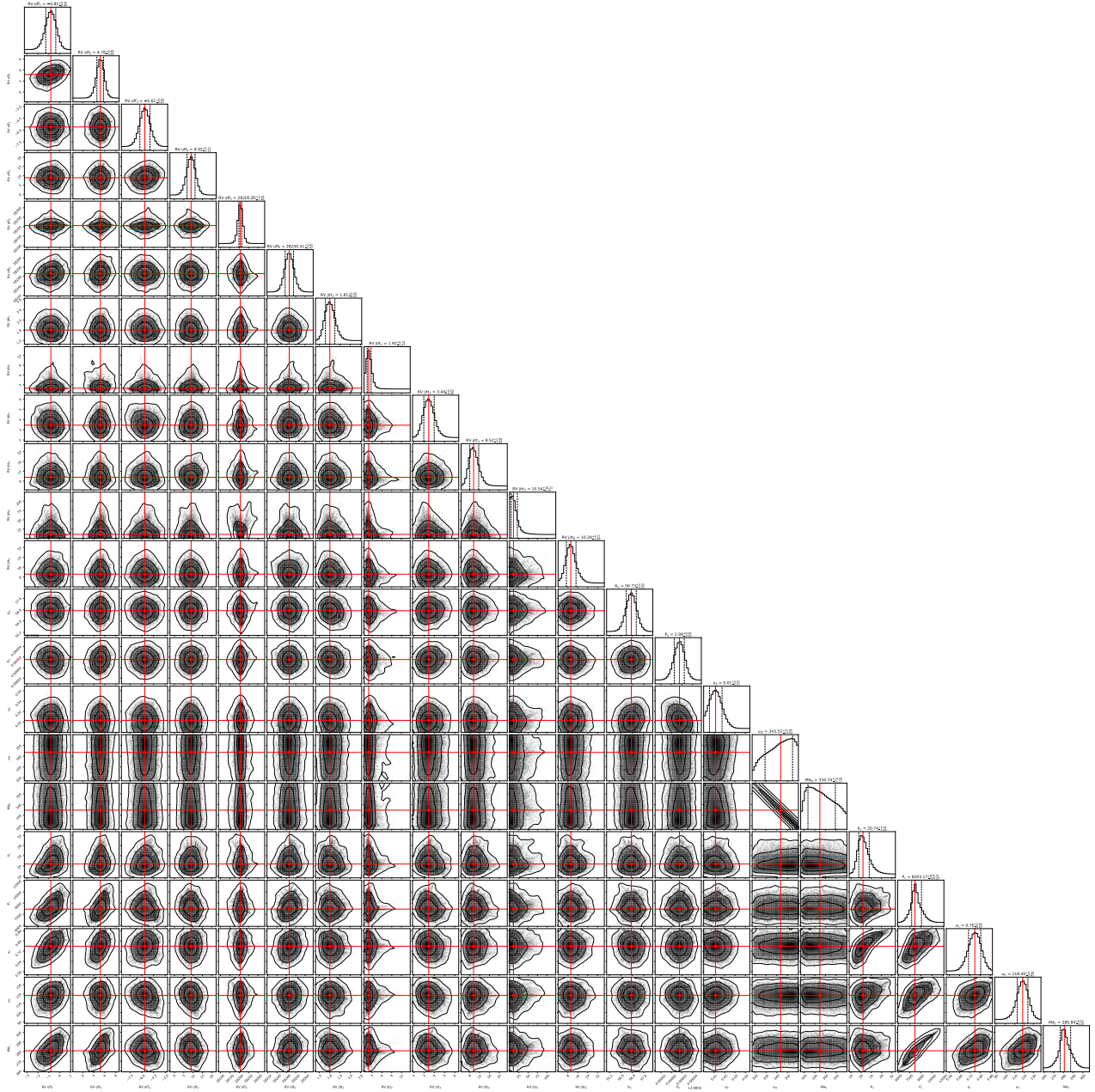


Figure 12. Corner plot - starting orbital period: 10000 days